Field evaluation of the installation and pullout of snakeskin-inspired anchorage elements

Alejandro Martinez[1,*], Ph.D., M. ASCE Fabian Zamora[2], Daniel Wilson[3], Ph.D., M. ASCE

[1]Civil and Environmental Engineering, University of California, Davis, CA 95616; Email: amart@ucdavis.edu
[2]Civil and Environmental Engineering, University of California, Davis, CA 95616; Email: fazamora@ucdavis.edu
[3]Civil and Environmental Engineering, University of California, Davis, CA 95616; Email: dxwilson@ucdavis.edu
*Corresponding author

Abstract

Soil nails and tieback anchors are extensively used for excavation support and slope stabilization; however, their performance can be complicated by limited pullout capacity or installation challenges. This paper presents the results of field load tests performed on anchorage elements with snakeskin-inspired surfaces that do not require grout and that can reduce the force required for installation. These tests evaluated the effect of the asperity geometry, soil type, and embedment depth on the anchor load transfer behavior and pullout capacity. The tests consisted of jacked installation and pullout loading in sites consisting of dense sand and structured silt. The test results in sand indicate that the installation force and pullout skin friction increase as the asperity height is increased and the asperity length is decreased. The pullout capacity of the snakeskin-inspired anchors was between 1.2 to 4.2 times greater than the capacity of a reference rough anchor. In the structured silt site, disturbance during installation influenced the pullout behavior, resulting in a decrease in anchor capacity as the asperity height was increased. However, the anchor capacity with small asperity heights was greater than that of the reference rough anchor. The snakeskin-inspired anchors mobilized direction-dependent skin friction, resulting in pullout skin friction values that were up to 3.0 and 4.5 times greater than those generated during installation in the sand

and silt sites, respectively, due to mobilized passive resistances during pullout. The results indicate that the snakeskin-inspired anchors can outperform conventional driven anchors in sands. However, the possible effects of installation disturbance should be carefully evaluated in sensitive, structured soils.

Keywords: ground anchors, soil anchors, snakeskin, pullout, bioinspiration

Introduction

Anchorage elements are extensively used for excavation support and slope stabilization. Tieback anchors and soil nails are commonly used in practice as part of earth retaining systems such as soil nail walls and soldier pile and lagging walls (Sabatini et al. 1999). Tieback anchors are pretensioned, whereas soil nails act passively. In soil nails, the movement of the soil wedge generates tensile loads that are resisted by the skin friction mobilized by the nail portion that extends past the wedge's failure surface. These anchorage elements offer advantages over other alternatives such as mechanically-stabilized earth retention walls and strut support systems because they do not require excavation and compaction of backfill, can be installed in a relatively short time with compact equipment, and can be more economical. Despite their benefits, soil nails and tieback anchors can suffer from limited anchorage capacity, leading to pullout that can result in excessive wall or slope movement, and challenges during installation such as grout migration.

Tieback anchors are predrilled and made of a steel bar that is grouted against the surrounding soil. Tieback anchors have an active bonding length with an enlarged diameter that is created by pressure-grouting and an unbonded length in which the steel bar can deform elastically (Sabatini et al. 1999). Traditionally, soil nails are installed by pre-drilling a hole into the backfill, inserting a bar, and grouting the nail (Lazarete 2015). The nails are typically made of steel or glass fiber-reinforced polymer (GFRP) and they can be either gravity- or pressure-grouted (Lazarete 2015; Zhu et al. 2011). Soil nails can also be inserted directly into the ground by driving, jacking, or rapid launching (Li et al. 2008; Sharma et al. 2019a; Steward and Ribera 1995).

The capacity of soil anchorage elements is mobilized either through skin friction or bearing capacity [Fig. 1]. Tieback anchors generate their capacity through skin friction and bearing resistance between the grout bulb at the end of the steel bar and the surrounding soil. Soil nails mobilize most of their capacity through friction between the nail and the surrounding soil (i.e., between grout, steel, or GFRP against soil). However, researchers have developed hybrid soil nails that also generate a significant portion of their capacity through bearing resistance mobilized by enlarged grouted bulbs created near the nail's end (Wang et al. 2017; Bhuiyan et al. 2020). The surface roughness and confining stress around a soil nail have controlling effects on its capacity. Specifically, nails with a rougher surface mobilize greater capacities due to the greater nail-soil interface friction angle and increases in the confining stress around the nail, leading to increases in capacity (Junaideen et al. 2004; Chu and Yin 2005; Tei et al. 2008; Sharma et al. 2019a).

The confining stress around an anchorage element can exceed the in-situ overburden stress due to densification of the surrounding soil during installation and soil dilation during shearing, which can be restricted by the surrounding soil. The latter effect is more pronounced in denser and more dilative soils and in elements with smaller diameters or rougher surfaces (Milligan and Tei 1998; Luo et al. 2000; Sharma et al. 2019b). Due to the dilation-induced increases in confining stress, the mobilized skin friction can exceed the calculated shear strength of the surrounding soil assuming a constant confining stress, leading to greater apparent friction coefficients or friction factors which tend to decrease with increasing overburden pressure due to the suppression of dilation (e.g. Luo et al. 2000). However, researchers have also reported no significant influence of overburden pressure on capacity in grouted soil nails, resulting from the decrease in confining stress during the drilling process (e.g. Zhang et al. 2009).

This paper investigates the effect of a specific type of surface texture on the behavior of jacked anchorage elements. Specifically, a series of field tests on anchorage elements with snakeskin-inspired surfaces were performed to investigate the behavior during jacking installation and subsequent loading, including their pullout capacity, overall load transfer behavior, and dependence of skin friction on the direction of loading. Experiments were performed on eight snakeskin-inspired anchors with different surface texture to evaluate the effect of the asperity height and length in sites composed of both dense sand and structured silt. The results of experiments on a reference rough anchor are used to evaluate the benefits of the snakeskin-inspired surface texture.

Previous work and basis for experimental design

Bio-inspired design involves adapting strategies employed by living organisms to address engineering challenges. In the last decade, geotechnical engineers have searched for solutions in nature for applications including anchorage elements and foundations, in-situ testing, slope stabilization, and tunneling (Martinez et al. 2022). Specifically relevant for soil-structure load transfer, the directional dependence of the friction generated between snakeskin and different substrates has been quantified by biologists, where relative displacement in the cranial direction (i.e., against the scales' sharp edges) generates greater friction coefficients than in the caudal direction (i.e., along the scales' mild slope) by factors between 1.4 and 3.0 (Gray and Lissmann 1950; Marvi and Hu 2012; Marvi 2013).

The field tests performed as part of this investigation were designed to build on previous research on snakeskin-inspired soil-structure interfaces. Martinez et al. (2019) and O'Hara and Martinez (2020) performed interface shear tests between surfaces generated based on the profiles of three preserved snake species [Fig. 2(a)] and two different sand types, where the surface asperities consisted of an asymmetric sawtooth pattern with a height of H and a length of L. The authors reported greater interface strengths in the cranial direction than in the caudal one [Fig. 2(b)]. Lee and Chong (2022), Vena Latha et al. (2022), and Stutz and Martinez (2021) reported similar differences between cranial and caudal interface friction angles. Interface shear tests with constant normal stiffness boundary conditions showed greater dilation-induced increases in normal effective stresses in the cranial direction caused by the greater interlocking between the snakeskin-inspired asperities and sand particles (O'Hara and Martinez 2020; O'Hara 2022) [Fig. 2(c)]. Laboratory tests have also shown the effect of the asperity height and length on tests with sand, where increases in H and decreases in L result in greater interface shear strengths, and in sand the L/H parameter has been shown to unify the interface strength trends [Fig. 2(d)]. The L/H ratio is related to the angle of the asperity during caudal shearing (i.e., smaller L/H indicates a larger angle) and to the normalized spacing between asperities during caudal shearing (i.e., smaller L/H indicates a smaller normalized spacing). Particle Image Velocimetry (PIV) analyses have shown the development of soil wedges ahead of the asperities during cranial shearing, suggesting transfer of load in the form of passive resistances (Martinez et al. 2019) [Fig. 2(e)].

Snakeskin-inspired surfaces have been implemented on piles with the purpose of enabling direction-dependent skin friction. O'Hara and Martinez (2022a) and Martinez and O'Hara (2021) performed centrifuge load tests on piles in loose and medium dense sands. Their results show a large difference in skin friction between piles installed in the caudal direction and pulled in the cranial direction and vice versa, with the cranial direction mobilizing greater skin friction in both installation or pullout [Fig. 2(f)]. For the caudally-installed and cranially-pulled pile, O'Hara and Martinez (2022a) reported a skin friction during pullout that was on average 40% greater than the skin friction during installation, likely resulting from greater increases in dilation-induced effective stresses around the pile. Zhong et al. (2021) performed 2D DEM simulations on a snakeskin-inspired pile, shedding light on the soil deformation and load transfer mechanisms involved in the mobilization of direction-dependent skin friction.

To the author's knowledge, field tests on geotechnical elements with snakeskin-inspired surfaces have not been reported in the literature. In this investigation, the behavior of anchors with snakeskin-inspired surfaces is explored with particular focus on the effect of the asperity height and length and soil type on the forces involved in the installation and pullout of the anchors. The results from field tests in dense sand are used to verify trends obtained from laboratory tests and centrifuge pile load tests. The tests on the structured silt site were performed to develop understanding of the behavior of the snakeskin-inspired anchors in a fine-grained soil with significant structure.

Materials and methods

Snakeskin-inspired anchors

Eight snakeskin-inspired anchors with different H and L were manufactured with stainless steel. The asperity height ranged from 0.5 to 4 mm while the asperity length ranged from 12 to 48 mm, yielding L/H ratios between 3 and 24 [Table 1, Figs. 3(a and b)]. The naming designation for the anchors is "HXLYY", where "X" represents the value of H in mm and YY represents the value of L in mm. For example, the H4L12 anchor has an H of 4 mm and an L of 12 mm.

The variations in H and L allowed evaluating their individual effects on the anchor load transfer behavior. Specifically, the H4L12, H2L12, H1L12, and H0.5L12 anchors have differences in H while keeping a constant L of 12 mm, whereas the H4L12, H4L24, and H4L48 and H2L12, H2L24, and H2L48 anchors have differences in L while maintaining a constant H of 4 and 2 mm, respectively. The anchors were machined in sections with a length of 152.4 mm for ease of manufacture, and the entire anchors were assembled to their final length using threaded studs [Fig. 3(b)]. Anchors with embedded lengths of 2.7 and 5.5 m were tested. All the anchors had an outer diameter of 22.3 mm. An additional reference anchor was tested to provide data representative of the behavior of a fully rough surface. The reference rough anchor consisted of a piece of #7 rebar with an outer diameter of 22.3 mm and the same length as the snakeskin-inspired anchors. The average and maximum surface roughness parameters of the rough anchor were measured as 0.613 and 1.755 mm, respectively, using a white light scanner. Considering the large surface roughness of the rough anchor, the interface friction angle can be considered to be equal to the surrounding soil's friction angle (i.e., $\delta = \varphi$ conditions, Martinez and Frost 2017). All the anchors were equipped with a section with the same diameter as the anchor (i.e., 22.3 mm) with a conical tip with an apex angle of 60° for protection and to reduce the penetration resistance.

Installation and load testing setup

All the anchor load tests were performed using a small, tracked drill rig equipped with a hydraulic actuator [Fig. 4(a)]. For ease of testing, all tests were performed on vertically-installed anchors. The anchors were installed by quasi-static jacking at a rate of about 2 cm/s using the drill rig's hydraulic actuator. A plate adapter was used to push a ball bearing that rested on the head of the anchors [Fig. 4(b)]. Three anchor sections were jacked with each stroke of the drill rig, for a penetration depth of about 460 mm per stroke. A centering frame was used to maintain verticality during installation of the anchors. Immediately after installation, the anchors were pulled using a chain hoist that was attached to the flanges at the end of the rig's hydraulic actuator [Fig. 4(c)] at a rate of about 2 cm/s. The installation and pullout forces were measured with a load cell installed at the head of the anchors, while the displacement of the anchors was measured using a string potentiometer attached to the bottom reference frame and the rig's hydraulic actuator. All the anchors were tested such that caudal shearing took place during installation to reduce the pushing forces and cranial shearing took place during pullout to increase the capacity. The reference rough anchor was not equipped with a load cell during installation; therefore, only pullout forces were measured for the tests on this anchor.

Test sites

The anchor load tests were performed at sites consisting of dense sand and structured silty soil. Nine anchor load tests at a target depth of 2.3 m were performed in the sand site while eighteen tests at depths of 2.7 and 5.5 m were performed in the structured silt site [Fig. 5]. The vertical effective stress (σ'_v) at the midpoint along the anchors' embedded length was around 22 kPa for the tests in the sand site and the corresponding σ'_v was around 24 and 48 kPa for the tests in the silty soil site with depths of 2.7 and 5.5 m, respectively.

The sand site consisted of a buried tank with a diameter and depth of 6.83 m filled with compacted concrete sand, and is referred to as the "sand pit". The sand was compacted in 10 cm thick lifts with a hand-operated compactor. Proctor compaction tests indicated a maximum dry unit weight of 20.5 kN/m^3 and an optimum water content of 7.5%. The sand was compacted to a target relative compaction of 95%, which was verified using a nuclear density gage and sand cone tests. The sand at the top of the tank was dry, while a small amount of moisture was present towards the bottom of the tank. However, there was no water table inside the sand pit. The sand had a median particle size of 0.75 mm, coefficient of uniformity of 5.0, coefficient of curvature of 0.8, less than 1% fines by mass, and maximum and minimum void ratios of 0.64 and 0.32, respectively.

The structured silt site was located next to the Center for Geotechnical Modeling in the UC Davis west campus near Putah Creek. Flooding events of the creek have led to significant layering, resulting in an appreciable degree of vertical and lateral spatial variability. Several wetting and drying events have overconsolidated the soil, resulting in a hard surficial layer. A Cone Penetration Test (CPT) revealed that the ground water table was located at a depth of 19.4 m. The soil is known locally as Yolo loam. The liquid and plastic limits of the Yolo loam at the testing site were measured as 34% and 23.5%, respectively. These values yield a classification of a low-plasticity silt (ML) based on the USCS soil classification system.

CPT soundings were performed in both sites to further characterize the soils in-situ. The sand pit showed CPT tip resistances (q_t) greater than 5 MPa at depths greater than 0.5 m [Fig. 6(a)]. The soil behavior index (I_C) was smaller than about 1.7, indicating clean dense to medium dense sands. The peak friction angle (φ'_p) was calculated using the Mayne (2006) correlation:

$$\varphi'_p = 17.6° + 11.0\,log\left[\frac{q_t/P_a}{\left(\sigma'_{v0}/P_a\right)^{0.5}}\right] \qquad \text{Eq. 1}$$

where P_a is the atmospheric pressure and σ'_{v0} is the overburden stress. Eq. 1 provides φ'_p values between 39° and 42°. The relative density (D_R) was calculated using the Jamiolkowski et al. (2003) correlation:

$$D_R = \frac{1}{2.90}\,ln\left[\frac{q_t/P_a}{17.74\left(\sigma'_{v0}/P_a\right)^{0.55}}\right] \qquad \text{Eq. 2}$$

Eq. 2 provides D_R values close to 90% at depths between 0.5 and 1 m which steadily reduce to about 70% at a depth of 4 m. The Mayne (2014) correlation was used to estimate an average total unit weight (γ_t):

$$\gamma_t = 26 - \frac{14}{1+[0.5\,log(f_s+1)]^2} \qquad \text{Eq. 3}$$

Eq. 3 yields an average γ_t of 19.4 kN/m^3.

Two CPT soundings in the Yolo loam site showed q_t magnitudes between 2 and 5 MPa that increased steadily with depth [Fig. 6(b)]. The I_C values are between 2.0 and 2.3 at depths smaller than 3 m, and they increase to about 2.5 at depths between 5 and 6 m, indicating a progression from sand mixtures to silt mixtures in the soil behavior type. The Mayne (2006) correlation yields near-constant friction angles with depth with values between 34° and 36°. The Mayne (2001) correlation was used to estimate preconsolidation stress values (σ'_p):

$$\sigma'_p = 0.33(q_t - \sigma'_{v0}) \qquad \text{Eq. 4}$$

The σ'_p were used to calculate overconsolidation ratios (OCR), indicating a highly overconsolidated crust and OCR values of about 2 at depths greater than 2.5 m. The Mayne (2014) correlation yielded an average total unit weight of 18.1 kN/m^3 in the Yolo loam. Comparison of the results of the two CPT soundings in the Yolo loam site shows an appreciable degree of variability in q_t, friction sleeve (f_s), I_C, and φ'_p; however, the quantities show consistent trends with increasing depth. Trendlines fitted to the q_t traces using polynomial functions are presented in Fig. 6 for both the sand pit and Yolo loam sites; these trendlines are used to estimate the penetration resistance of the anchors in the analysis presented in the following sections.

Results

The transfer of load between the anchors' asperities and the surrounding soil takes place in both friction and passive modes due to the geometry of the snakeskin-inspired asperities. During installation in the caudal direction, shear ($F_{S,i}$) and normal ($F_{N,i}$) forces are mobilized against the surface of any given asperity, producing a resultant force ($F_{R,i}$) [Fig. 7(a)]. These forces can be translated into vertical ($F_{VS,i}$) and horizontal forces ($F_{HS,i}$) using the following equations:

$$F_{VS,i} = F_{N,i} \sin\alpha + F_{S,i} \cos\alpha \qquad \text{Eq. 5}$$

$$F_{HS,i} = F_{N,i} \cos\alpha + F_{S,i} \sin\alpha \qquad \text{Eq. 6}$$

where α is the angle between the asperity surface and the vertical direction. The measured force at the anchor head consists of the sum of the vertical installation forces at each asperity ($F_{VS,I,i}$) and the force mobilized at the anchor's tip section ($F_{VT,I}$). Note that since the tip section has a length of 10 mm behind the shoulder; therefore a frictional component can be mobilized in addition to the penetration resistance component [Fig. 7(b), Eq. 7].

$$Installation\ force = \sum_{i=1}^{N_A} F_{VS,I,i} + F_{VT,I} \qquad \text{Eq. 7}$$

During pullout in the cranial direction, an additional passive component is mobilized due to the annular bearing area of the asperities. The measured force at the anchor head consists of the sum of the vertical pullout ($F_{VS,P,i}$) and passive forces ($F_{PA,P,i}$) at each asperity and some friction mobilized at the anchor tip section [Fig. 7(c), Eq. 8].

$$Pullout\ force = \sum_{i=1}^{N_A} F_{VS,P,i} + \sum_{i=1}^{N_A} F_{PA,P,i} + F_{VT,P} \qquad \text{Eq. 8}$$

In the following sections, the data is analyzed in terms of the average penetration forces, peak pullout capacities, pullout stiffnesses, and pullout softening rates. Tables 2 and 3 present a summary of the test results. The pullout capacity is quantified in terms of the ratio of the average shear stress to average vertical effective stress (τ_s/σ'_v), where the former is calculated as the total measured pullout force divided by the anchor's surface area and the latter is calculated as the average value along the anchor's length. The vertical projection of the anchor surface area is considered for the calculation of τ_s, consisting of the anchor circumference by its embedded length. τ_s/σ'_v values are used for comparison rather than τ_s magnitudes to enable comparison of the results of anchors that were fully embedded with those that reached installation refusal at smaller depths in the sand site, as described below. It should be noted that a more appropriate normalization would use the horizontal effective stress (σ'_h). However, since measurements of σ'_h were unfeasible during this investigation, σ'_v was used in the normalization. The pullout stiffness (k_{50}) is defined as the slope of the pullout curve from the origin to a force equivalent to half of the peak capacity and represents the rate of capacity mobilization at small displacements [Fig. 7(d)]. The softening rate (S_t) is defined as the slope of the pullout curve over a displacement of either 100 mm or 2L after the peak load is mobilized [Fig. 7(d)] and represents the rate at which capacity is degraded past the peak (i.e., failure brittleness).

Tests in the sand pit site

Nine load tests were performed at the sand pit site. The reported trends are compared with those from previously published studies consisting of laboratory interface shear tests and centrifuge pile load tests against sands.

Installation of anchors

The total measured force during anchor installation increased with depth due to both the increases in anchor surface area and vertical effective stress, and is influenced by the asperity height and length of the snakeskin-inspired texture. Fig. 8(a) presents the installation forces as a function of the anchor tip depth, showing an increase in magnitude as H was increased, where H is varied from 0.5 to 4 mm while L is maintained constant at 12 mm. As shown, the H4L12 anchor mobilized the greatest forces while the H0.5L12 anchor produces the smallest magnitudes. In fact, refusal was reached at a depth of 1.32 m for the H4L12 due to the high installation forces and limited reaction mass of the drill rig. The installation forces decreased as L was increased for H values of 4 and 2 mm, as shown in Figs. 8(b and c). In both test series, the anchors with an L of 12 mm generated the greatest total forces while the anchors with an L of 48 mm produced the smallest forces. The asperity geometry affects the skin friction force, but does not influence the penetration resistance force as previously shown by O'Hara and Martinez (2022b) during centrifuge pile load tests in sand. Assuming that the anchors' tip resistance is equal to the q_t measured during CPT soundings allows calculating the tip penetration force. Then, the skin friction force can be calculated by subtracting the tip penetration force from the total head force. Figs. 8(d–f) presents the traces of the skin friction forces as a function of depth. The skin friction force follows the same trends with H and L as described for the total force, and accounts for 18 to 70% of the total installation force. The anchors with greater H and smaller L mobilized greater fractions of the total installation force. Figs. 8 (g-i) show the calculated average stress ratios which exhibit a rapid decrease at shallow depths and stabilize at depths greater than about 1.3 m. This decrease is due to the gradual densification of sand it continues to be sheared by the snakeskin-inspired asperities passing, as it has been previously reported for piles (White and Lehane 2004). The decrease in τ_s/σ'_v is also likely due to the suppression of dilation due to the increasing overburden stress.

The effect of H on the installation forces is more pronounced than that of L on the skin friction. Namely, the skin friction force is about 12 times greater in the H4L12 anchor than the

H0.5L12 anchor, while the skin friction is only about 2 times greater in the H4L12 and H2L12 anchors than the H4L48 and H2L48 anchors, respectively. Figs. 9(a and b) show the stress ratios at a depth of 1.3 m, where the effects of H and L are decoupled. Individual relationships can be drawn as a function of H for different L values [Fig. 9(a)] or as a function of L for different H values [Fig. 9(b)]. Plotting the τ_s/σ'_v values as a function of the L/H ratio appears to unify the data reasonably well [Fig. 9(c)], in agreement with results of laboratory tests on sands from Martinez et al. (2019) in both the caudal and cranial directions as shown in Fig. 2(d). The relationship between τ_s/σ'_v and L/H can be fitted with a power law function, indicating a greater sensitivity of at smaller L/H values.

Pullout of anchors

The pullout response of the anchors is analyzed in terms of the τ_s/σ'_v ratio due to differences in final anchor embedment depth, particularly for the H4L12 anchor which reached refusal at a relatively shallow depth. An additional test on the reference rough anchor is included for comparison. The pullout response was measured over a vertical displacement of 200 mm, or 9 times the anchor diameter [Figs. 10(a–c)].

The pullout capacity was influenced by the asperity geometry. Specifically, increases in H led to sharp increases in τ_s/σ'_v, as shown in Fig. 10(a) for anchors with a constant L of 12 mm. For this value of L, all the snakeskin-inspired anchors mobilized greater pullout capacities than the reference rough anchor. Particularly, the H4L12, H2L12, H1L12, and H0.5L12 anchors mobilized peak τ_s/σ'_v that are 4.2, 1.8, 1.4, and 1.2 times greater than the reference rough anchor. For a constant H, increasing L led to a decrease in τ_s/σ'_v and to a change in the shape of the pullout curve [Figs. 10(b and c)]. Specifically, the pullout curves of the anchors with a small L of 12 mm show an initial stiff response up to the peak τ_s/σ'_v followed by strain softening, while the pullout response of the anchors with an L of 48 mm show an initially softer response with a capacity that continues to increase with increasing displacement. The peak capacity of all the snakeskin-inspired anchors was greater than that of the reference rough anchor; however, the H2L48 anchor exhibited a significantly softer response than the rough anchor.

The asperity height and length had distinct effects on the peak stress ratio, with H having a greater influence on the magnitude of peak τ_s/σ'_v [Figs. 11(a and b)]. Namely, an increase in H from 0.5 to 4 mm for an L of 12 mm led to an increase in peak τ_s/σ'_v of 340%, while an increase in L from 12 to 48 mm for H values of 4 and 2 mm led to increases in peak τ_s/σ'_v of 220% and 160%, respectively. The L/H ratio unifies the peak τ_s/σ'_v data showing greater sensitivity at smaller L/H values; this relationship can be reasonably well fitted with a power law function, similarly to the installation skin friction forces. The trend between peak τ_s/σ'_v and L/H is also in agreement with laboratory cranial shearing results on sands presented by Martinez et al. (2019), as shown in Fig. 2(d). The three figures show the greater pullout capacity of all the snakeskin-inspired anchors in comparison with the reference rough anchor.

The stiffness and softening rates of the snakeskin-inspired anchor were generally greater than that of the reference rough anchor. While H does not appear to affect k_{50} in a systematic manner, anchors with smaller L produced stiffer responses [Figs. 12(a and c)]. The data also shows a decrease in k_{50} with increasing L/H [Fig. 12(e)]. The anchors with small L/H mobilized stiffnesses between 1.8 and 2.6 times greater than the reference rough anchor, while the k_{50} values were close between the rough anchor and the snakeskin anchors with L/H of 24. The softening rate was determined using a displacement of either 100 mm or 2L after the peak load, but there are no systematic differences in the calculated S_t values. There is no clear relationship between S_t and either H and L. However, a trend emerges when plotted in terms of L/H, with larger S_t for small L/H and an apparent convergence of the softening rates of the snakeskin and reference rough anchors at large L/H values.

Tests in the Yolo loam site

Eighteen tests were performed at the Yolo loam sites at two different target depths. These tests were performed to build on the existing tests on snakeskin-inspired surfaces, which have been primarily performed against dry sands.

Installation of anchors

The total force and skin friction force of the anchors in the Yolo loam site showed significant variation, likely due to the spatial variability in the site. Figs. 13(a–i) show the total force, skin friction force, and stress ratio distributions with depth for the anchors installed to a depth of 2.7 m. For certain anchors, the total and skin friction forces were relatively constant with depth (i.e., H2L12, H2L24), while for other anchors the installation forces were greatest at shallow depths due to the presence of the shallow overconsolidated crust at the site (i.e., H4L12, H4L24, H2L48). This results in decreases in τ_s/σ'_v with depth which stabilize at depths greater than about 1.5 m. The depth traces for the anchor tests installed to a depth of 5.5 m are not presented for brevity; however, they follow similar trends with near-constant forces with depth or large forces at shallow depths.

In general, the installation stress ratios decreased as the asperity height was increased, and changes in asperity length did not lead to systematic changes in the skin friction force, as shown in Figs. 14(a–c). The trend with H is particularly clear for the anchors installed to a depth of 2.7 m, while the deeper tests show a significant amount of variability. This decrease in force with H shows the opposite trend to the anchor tests in the sand pit site. This is due to the structure of the Yolo loam at the site, where the overconsolidated and unsaturated state leads to a stiff yet brittle behavior, making the soil sensitive to disturbance. As described in more detail in the next section, the anchors with greater H led to greater disturbance of the soil which reduced the amount of skin friction at locations away from the anchors' tip. This is particularly evident for the H4L24 anchor which mobilized a skin friction of nearly zero. When plotted as a function of L/H, no clear trends emerge with τ_s/σ'_v [Fig. 14(d)]. The results also show that the stress ratios are generally greater for the shallower anchors, likely due to the aforementioned disturbance. Overall, the installation forces are controlled by the spatial variability of the site and the sensitivity of the structured silty soil.

Pullout of anchors

The asperity height had a greater influence on the pullout capacity and stress ratio – displacement curves than the asperity length in the structured silt. Figs. 15(a and b) show the pullout curves at depths of 2.7 and 5.5 m, respectively, for anchors where H is varied and L is kept at 12 mm. The pullout curves for the anchor with the smallest H of 0.5 mm show a peak capacity followed by strain softening, while the curves for the anchors with greater H and L did not show clearly defined peak capacities. The results show an increase in τ_s/σ'_v as the H is reduced. Photographs from anchors fully pulled out of the ground can explain this trend. For the anchors with a large H, the structured silty soil is disturbed during installation, offering little resistance during pullout, as evident in the photograph in Fig. 16(a) showing loose soil clumps ahead of the asperities. In contrast, the anchor with a small H produces a smaller amount of disturbance during installation, resulting in soil-soil shearing during the pullout test. This behavior contrasts with that observed in the sand pit tests due to the sand's ability to flow around the asperity. The field tests show passive wedges developed ahead of the asperities during pullout loading [Fig. 16(b)], in agreement with previous laboratory tests (i.e., Fig. 2(e)). In this case, the greater bearing area of the asperities with a larger H leads to a greater pullout resistance.

The peak anchor capacity decreased sharply with increasing H, as shown in Fig. 17(a). The relationship between $\tau_{s,peak}/\sigma'_v$ and H can be fitted with a power function for the tests at both depths. The asperity length did not have a systematic effect on the $\tau_{s,peak}/\sigma'_v$, resulting in significant scatter in the relationship with the L/H ratio [Figs. 17(b–d)]. The anchors with H of 0.5 and 1 mm mobilized greater $\tau_{s,peak}/\sigma'_v$ than the reference rough anchor. Specifically, the $\tau_{s,peak}/\sigma'_v$ is 2.5 to 4.4 times greater for the H0.5L12 anchor than the reference anchor, while the H1L12 anchor mobilized a $\tau_{s,peak}/\sigma'_v$ that is between 1.4 and 1.7 times greater than the reference anchor. It is noted that results on the stiffness and sensitivity of the anchor load tests in the Yolo loam site are not included because many of the curves did not reach a distinct peak τ_s/σ'_v.

Discussion

Directionality

A unique aspect of the snakeskin-inspired texture is its ability to mobilize different interface strengths in the cranial and caudal directions. These differences are driven by differences in the interactions between the asperities and soil, where the bearing area in the cranial direction produces passive resistances in addition to frictional load transfer. In the caudal direction, the load of transfer is likely dominated by shearing between the steel and soil, while some passive resistances can be mobilized particularly when the asperity slope is large (i.e., small L/H).

The difference in skin friction can be quantified in terms of the ratio of the peak pullout skin friction force (i.e., in the cranial direction) to the peak installation skin friction force (i.e., in the caudal direction). The skin friction directionality is presented in Figs. 18(a and b) for the tests in the sand site and in Figs. 18(c and d) for the tests in the structured silt site. As shown, the directionality decreases as the asperity height increases in both soil types, and the relationships can be fitted with power functions. For an H of 0.5 mm, the directionality is close to 3 in the sand and between 2.3 and 4.5 in the structured silt. At an H of 4 mm, the directionality is around 1.8 in the sand, while in the structured silt the directionality is smaller than 1.0, indicating a greater skin friction during installation likely as a result of soil disturbance as previously described. The directionality increases with an increase in the L/H ratio in both sites; however, the results from the silt site show a significant amount of scatter. Overall, the results show that the skin friction directionality has a well-behaved relationship with H.

Load transfer

The snakeskin-inspired pattern results in transfer of load in the form of passive resistances and skin friction, leading to the large capacities observed during the field tests. This effect is particularly pronounced during cranial shearing due to the bearing area of the asperities. Measurements of soil deformation during laboratory tests confirm this, where soil wedges are displaced during cranial shearing indicating local passive conditions [Fig. 2(e)].

The peak stress ratio values measured during the tests in the sand pit site can be used to further examine the likely load transfer mechanisms between the snakeskin-inspired asperities and the surrounding soil. Assuming a purely frictional transfer of load, as typically done for the design of piles, would lead to calculation of the skin friction as $\tau = \sigma'_h \times \tan(\delta') = \sigma'_v \times K \times \tan(\delta')$, where σ'_h is the horizontal effective stress against the anchor surface, K is the lateral earth pressure coefficient, and δ' is the interface friction angle (Salgado 2006). Assuming $\delta' = \varphi'_p$ for a rough interface, according to Uesugi and Kishida (1986), allows back-calculating the in-situ K coefficients. Using an average φ'_p of 41° from the CPT results [Fig. 6(a)] yields K coefficients mobilized at peak conditions of 12.7 and 7.7 for the H4L12 and H4L24, which are unreasonably high for axially-loaded elements. For example, finite element analyses from Salgado (2006) yield K values between 2.0 and 5.5 for piles in sand with a D_R of 80%. The back-calculated K values for the anchor with the smallest H (i.e., H0.5L12) and the reference rough anchor are 3.8 and 3.0, respectively, falling in the typical range for high D_R sands. This suggests that passive resistances contribute significantly to the transfer of load, particularly for textures with high H values. However, it should be considered that the small diameter of the anchors could also result in dilation-induced increases in horizontal effective stresses, as described by Luo et al. (2000) and Junaideen et al. (2004), contributing to the large back-calculated K values.

The asperity height, length, or L/H ratio were shown to control different aspects of the anchor pullout response in sand. Increases in H led to greater increases in peak capacity than increases in L. For example, a fourfold increase in H from 1 to 4 mm led to an increase in peak capacity by a factor of 3.0 while a fourfold decrease in L from 48 to 12 mm, translated to a corresponding increase in the number of asperities, led to an increase in peak capacity by a factor between 2.2 and 1.6. This difference cannot be explained simply by the increases in the total annular bearing area, as increasing H leads to an increase in annular bearing area by a factor of 3.4 while decreasing L leads to an increase by a factor of 4.0. Rather, it is possible that the bearing area magnitude at each asperity is the controlling factor. Namely, a greater H may allow the individual asperities to fully develop passive conditions, thus inducing local increases in effective stresses. It is noted that while a similar effect has been reported for other applications, such as screw anchors, multi-plate anchors, and self-burrowing probes (e.g., Luttenegger 2011; Nelly and

Hambleton 2019; Chen et al. 2022), these have much larger sizes compared to the soil particle sizes. Therefore, the influence of particle size effects, should be assessed in the future. The initial anchor stiffness was mostly influenced by L, suggesting that the number of asperities, rather than their height, controls this parameter, possibly because at small displacements the passive resistances have not been fully mobilized. Lastly, the softening rate was shown to increase with L/H, which in cranial shearing represents the normalized spacing between asperities. This trend may be explained by the interaction between asperities if it is considered that each asperity disturbs soil within a zone locally around it which grows with pullout displacement. In sand, this disturbance likely causes exhaustion of the soil's dilative potential and thus softening. Therefore, as the displacement is increased, the zones may begin to overlap, producing an overall softening anchor response.

Applicability of snakeskin-inspired anchors in different soil types

The results of the field tests highlight the applicability of the anchors with snakeskin-inspired texture in different soil types. In the sandy soils, all the tested snakeskin-inspired anchors outperformed the reference rough anchor, in some instances by factors as high as 4 in terms of the peak pullout capacity. In contrast, the pullout performance of the snakeskin-inspired anchors in the structured silt was controlled by the disturbance caused during installation. This led to the snakeskin-inspired anchors generating greater pullout capacities than the reference rough anchor when the H was small, but their capacity was smaller than that of the reference rough anchor when H was large. The increase in capacity with H in sandy soils is in agreement with previously published results from laboratory interface shear tests and centrifuge pile load tests (Martinez et al. 2019; O'Hara and Martinez 2020; O'Hara and Martinez 2022a). However, this comes at the cost of increased installation forces. For application in sensitive soils such as the structured silt in the Yolo loam site, careful evaluation is required to evaluate the possibility of detrimental effects of installation disturbance. All anchors were tested at effective stress levels that at the lower limit of magnitudes relevant for slope stabilization and excavation support. Therefore, future studies should focus on understanding the possible effects of increased overburden stress and depth on the installation and pullout responses.

This field testing campaign did not include tests in saturated, normally consolidated clay. However, the results of interface shear tests from Huang and Martinez (2021) suggest that the snakeskin-inspired texture can produce beneficial behaviors in this soil type. Namely, the laboratory results indicate shearing in the cranial direction generates greater skin friction than in the caudal direction. In addition, the ability of soft clay to flow around asperities will likely lead to limited installation disturbance effects.

Implications in geotechnical practice and future deployment

One of the main benefits of driven or launched soil nails or anchors is that grout is not needed, leading to faster production and simpler logistics because fewer steps and equipment are needed for installation. Another benefit of the snakeskin-inspired anchors is their greater capacity. Namely, the H4L12 anchor in the sand pit site mobilized 4.2 times the peak capacity of the reference rough anchor, while the H0.5L12 anchor in the Yolo loam site mobilized between 2.5 and 4.4 times the peak capacity of the reference rough anchor. For a project, this would mean that either fewer anchors or anchors with smaller lengths would be needed to provide the required pullout capacity, resulting in material and installation time savings.

The forces involved can be significantly greater during anchor pullout than during installation. For example, the ratio of the total pullout force to total installation force, which also accounts for the tip penetration resistance, is greater than or equal to one for all tests in the sand pit, indicating that in terms of total net force, the anchors require a greater force to fail in tension than to be jacked into the ground. The anchors with a small H have a greater total force ratio, with the H0.5L12 anchor mobilizing about twice the pullout force compared to the total installation force. The direction-dependent behavior of the snakeskin-inspired anchors can allow for installation with smaller forces compared to a conventional rough anchor, potentially allowing for the use of smaller installation equipment further providing efficiency in the logistics at project sites and potentially reducing the cost and environmental impacts.

The snakeskin-inspired anchors were machined in a lathe in sections with a length of about 150 mm. Because of this specialty machining, the anchor prototypes tested in this investigation have a high cost. In addition, the need to assemble the anchors results in a relatively slow installation in comparison with installation of an anchor composed of a single piece. In the future, the snakeskin-inspired anchors could become a competitive technology if their benefits in capacity and installation procedures outweigh the possible additional costs of manufacturing.

Conclusions

A series of field load tests were performed on anchorage elements with snakeskin-inspired surfaces in two sites composed of dense sand and structured, overconsolidated low-plasticity silt at two different depths. The snakeskin-inspired surfaces have previously been shown to mobilize direction-dependent skin friction, where shearing in the cranial direction mobilizes greater strength than in the caudal direction. The goal of these tests was to evaluate the effect of the asperity height and length on the forces involved in the installation and pullout of the snakeskin-inspired anchors, compare the results with those of a reference "fully rough" anchor, and quantify the direction-dependence of the anchor skin friction. Load tests were performed on eight different snakeskin-inspired anchors to discern the effect of the asperity height and length.

The skin friction during installation and pullout was highly influenced by the asperity height and length in the tests performed in the sand site. During both test stages, increasing the asperity height for any given length and decreasing the asperity length for any given height led to large increases in skin friction. The ratio of asperity length to height (i.e., L/H) unified the installation skin friction and peak pullout capacity data in relationships that can be fitted with power functions. The skin friction during pullout loading of all the snakeskin-inspired anchors was greater than that mobilized by the fully rough anchor by factors as high as 4.2. The asperity length and L/H ratio controlled the initial stiffness of the anchors, with a decrease in stiffness with an increase in either parameter. The post-peak softening rate decreased as the L/H ratio was increased, indicating that while the anchors with small L/H mobilize greater capacities and initial stiffness, their capacity can reduce with continued deformation.

In the structured silt site, the skin friction during installation and pullout generally decreased with an increase in asperity height. Due to the sensitivity of the material, the snakeskin-inspired anchors with taller asperities produced a greater degree of disturbance during installation, which resulted in a reduction of the pullout capacity. This led to a decrease in pullout capacity as the asperity height was increased. Still, the snakeskin-inspired anchors with small asperity heights of 0.5 and 1 mm mobilized greater capacities than the reference rough anchor.

The anchors mobilized significant skin friction directionality during the field tests. The skin friction directionality was defined as the ratio of the peak pullout to peak installation skin friction forces. The directionality decreased as the asperity height was increased and as the L/H ratio was increased. Directionality values were mobilized between 2.9 and 1.8 in the sand site and between 4.5 and 0.3 in the structured silt site. The directionality is a result of the difference in load transfer mechanisms, where greater passive resistances are mobilized during cranial pullout due to the bearing area produced by the asperities.

The greater capacity of the snakeskin-inspired anchors can result in a reduction in the anchor length or the number of anchors needed to mobilize a required pullout capacity. The direction-dependence of the mobilized skin friction can allow for installation of anchors that mobilize a greater pullout capacity for a specific jacking installation force or that require smaller installation forces to generate a specific pullout capacity. These aspects can benefit projects by simplifying their logistics and potentially resulting in reduction of cost and environmental impacts. Future efforts should be devoted to producing designs of the snakeskin-inspired anchors that use available materials to simplify their installation and reduce their cost.

Data Availability Statement

Raw data that support the findings of this study are available from the corresponding author, upon reasonable request.

Acknowledgements

This material is based upon work supported by the Engineering Research Center Program of the National Science Foundation under Cooperative Agreement No. EEC-1449501 and by the National Science Foundation (NSF) under Award No. 1942369. The load tests were made possible due to support from the UC Davis CGM, which is supported under grant No. CMMI-1520581.

The donation of in-kind services by Conetec Inc. for the performance of CPT soundings is gratefully acknowledged. Any opinions, findings and conclusions expressed in this material are those of the author(s) and do not necessarily reflect those of the NSF. The assistance of Chad Justice during the field tests is greatly appreciated.

References

Bhuiyan, M. Z. I., Wang, S., & Carter, J. P. (2021). Experimental study of an innovative driven and grouted soil nail (x-Nail). *Canadian Geotechnical Journal*, *58*(8), 1205–1215. https://doi.org/10.1139/cgj-2020-0084

Chen, Y., Martinez, A., & DeJong, J.T. (2022). DEM simulations of a bio-inspired site characterization probe with two anchors. Accepted for publication in *Acta Geotech.* https://doi.org/10.1007/s11440-022-01684-5.

Chu, L.-M., & Yin, J.-H. (2005). Comparison of Interface Shear Strength of Soil Nails Measured by Both Direct Shear Box Tests and Pullout Tests. *Journal of Geotechnical and Geoenvironmental Engineering*, *131*(9), 1097–1107. https://doi.org/10.1061/(ASCE)1090-0241(2005)131:9(1097)

David Suits, L., Sheahan, T., Yin, J.-H., & Su, L.-J. (2006). An Innovative Laboratory Box for Testing Nail Pull-Out Resistance in Soil. *Geotechnical Testing Journal*, *29*(6), 100216. https://doi.org/10.1520/GTJ100216

Gayathri, V. L., Vangla, P., & Riya, A. (2022). Effect of snakeskin-inspired patterns on the shear response of soil—Continuum interfaces. *International Journal of Geotechnical Engineering*, *16*(6), 759–775. https://doi.org/10.1080/19386362.2022.2066049

Gray, J., & Lissmann, H. W. (1950). The kinetics of locomotion of the grass-snake. *Journal of Experimental Biology, 26(4), 354-367*. https://doi.org/10.1242/jeb.26.4.354

Huang, L., & Martinez, A. (2021). Load Transfer Anisotropy at Snakeskin-Inspired Clay-Structure Interfaces. *IFCEE 2021*, 119–129. https://doi.org/10.1061/9780784483428.013

Jamiolkowski, M., Lo Presti, D.C.F., & Manassero, M (2003). Evaluation of Relative Density and Shear Strength of Sands from CPT and DMT. Soil Behavior and Soft Ground Construction, 201-238.

Junaideen, S. M., Tham, L. G., Law, K. T., Lee, C. F., & Yue, Z. Q. (2004). Laboratory study of soilnail interaction in loose, completely decomposed granite. *Canadian Geotechnical Journal*, *41*(2), 274–286. https://doi.org/10.1139/t03-094

Lazarete, C.A., Elias, V., Esponiza, R.D., & Sabatini, P.L. (2003). *Geotechnical Engineering Circular No. 7, Soil Nail Walls (FHWA A0-IF-03-017)*. Federal Highway Administration.

Lee, S.-H., & Chong, S.-H. (2022). A Study on Friction Anisotropy between Sand and Surface Asperities of Plate Using Modified Direct Shear Test. *Journal of the Korean Geotechnical Society*, *38*(2), 29–38. https://doi.org/10.7843/KGS.2022.38.2.29

Li, J., Tham, L. G., Junaideen, S. M., Yue, Z. Q., & Lee, C. F. (2008). Loose Fill Slope Stabilization with Soil Nails: Full-Scale Test. *Journal of Geotechnical and Geoenvironmental Engineering*, *134*(3), 277–288. https://doi.org/10.1061/(ASCE)1090-0241(2008)134:3(277)

Luo, S. Q., Tan, S. A., & Yong, K. Y. (2000). Pull-Out Resistance Mechanism of a Soil Nail Reinforcement in Dilative Soils. *Soils and Foundations*, *40*(1), 47–56. https://doi.org/10.3208/sandf.40.47

Lutenegger, A. (2011). Behavior of multi-helix screw anchors in sand. *Proc. 2011 Pan American Geotechnical Conference.*

Martinez, A. (2021). Skin Friction Directionality in Monotonically- and Cyclically-Loaded Bio-inspired Piles in Sand. *DFI Journal The Journal of the Deep Foundations Institute*, *15*(1). https://doi.org/10.37308/DFIJnl.20200831.222

Martinez, A., DeJong, J., Akin, I., Aleali, A., Arson, C., Atkinson, J., Bandini, P., Baser, T., Borela, R., Boulanger, R., Burrall, M., Chen, Y., Collins, C., Cortes, D., Dai, S., DeJong, T., Del Dottore, E., Dorgan, K., Fragaszy, R., … Zheng, J. (2022). Bio-inspired geotechnical engineering: Principles, current work, opportunities and challenges. *Géotechnique*, *72*(8), 687–705. https://doi.org/10.1680/jgeot.20.P.170

Martinez, A., & Frost, J. D. (2017). The influence of surface roughness form on the strength of sand–structure interfaces. *Géotechnique Letters*, *7*(1), 104–111. https://doi.org/10.1680/jgele.16.00169

Martinez, A., Palumbo, S., & Todd, B. D. (2019). Bioinspiration for Anisotropic Load Transfer at Soil–Structure Interfaces. *Journal of Geotechnical and Geoenvironmental Engineering*, *145*(10), 04019074. https://doi.org/10.1061/(ASCE)GT.1943-5606.0002138

Marvi, H. (2013). *The Role of Functional Surfaces in the Locomotion of Snakes.* Doctoral dissertation, Georgia Institute of Technology.

Marvi, H., & Hu, D. L. (2012). Friction enhancement in concertina locomotion of snakes. *Journal of The Royal Society Interface*, *9*(76), 3067–3080. https://doi.org/10.1098/rsif.2012.0132

Mayne, P. W. (2001). *Stress-strain-strength-flow parameters from enhanced in-situ tests*.

Mayne, P. W. (2014). *Interpretation of geotechnical parameters from seismic piezocone tests*.

Mayne, P. W. (2006). The Second James K. Mitchell Lecture Undisturbed sand strength from seismic cone tests. *Geomechanics and Geoengineering*, *1*(4), 239–257. https://doi.org/10.1080/17486020601035657

Milligan, G.W.E., & Tei, K. (1998). The Pull-Out Resistance of Model Soil Nails. *Soils and Foundations, 38(2), 179-190.*

Nally, A. & Hambleton, J.P. (2019) Assessment of analysis techniques for multi-plate anchors in sand. *Proc. 44th annual conference on deep foundations.*

Ng, C. W. W., & Lee, G. T. K. (2002). A three-dimensional parametric study of the use of soil nails for stabilising tunnel faces. *Computers and Geotechnics*, *29*(8), 673–697. https://doi.org/10.1016/S0266-352X(02)00012-5

O'Hara, K. B., & Martinez, A. (2020). Monotonic and Cyclic Frictional Resistance Directionality in Snakeskin-Inspired Surfaces and Piles. *Journal of Geotechnical and Geoenvironmental Engineering*, *146*(11), 04020116. https://doi.org/10.1061/(ASCE)GT.1943-5606.0002368

O'Hara, K. B., & Martinez, A. (2022a). Load Transfer Directionality of Snakeskin-Inspired Piles during Installation and Pullout in Sands. *Journal of Geotechnical and Geoenvironmental Engineering*, *148*(12), 04022110. https://doi.org/10.1061/(ASCE)GT.1943-5606.0002929

O'Hara, K. B., & Martinez, A. (2022b). Shaft and Base Capacity of Snakeskin-Inspired Piles from Centrifuge Pile Tests. *Geo-Congress 2022*, 170–180. https://doi.org/10.1061/9780784484029.016

O'Hara, K.B. (2022). *A Multiscale Study of the Interface Behavior between Sand and Snakeskin-inspired Surfaces and Pile Shafts*. Doctoral dissertation, University of California Davis.

Pradhan, B., Tham, L. G., Yue, Z. Q., Junaideen, S. M., & Lee, C. F. (2006). Soil–Nail Pullout Interaction in Loose Fill Materials. *International Journal of Geomechanics*, *6*(4), 238–247. https://doi.org/10.1061/(ASCE)1532-3641(2006)6:4(238)

Sabatini, P.J., & Bachus, R.C. (1999). *Geotechnical Engineering Circular No. 4: Ground Anchors and Anchored Systems (FHWA-IF-99-015).* Federal Highway Administration.

Salgado, R. (2006). *The Engineering of Foundations.* McGraw Hill.

Sharma, M., Samanta, M., & Punetha, P. (2019). Experimental Investigation and Modeling of Pullout Response of Soil Nails in Cohesionless Medium. *International Journal of Geomechanics*, *19*(3), 04019002. https://doi.org/10.1061/(ASCE)GM.1943-5622.0001372

Sharma, M., Samanta, M., & Sarkar, S. (2019). Novel Laboratory Pullout Device for Conventional and Helical Soil Nails. *Geotechnical Testing Journal*, *42*(5), 20170319. https://doi.org/10.1520/GTJ20170319

Sharma, M., Samanta, M., & Sarkar, S. (2020). A study on interface shear behaviour of soil nails from pullout and direct shear tests. *International Journal of Physical Modelling in Geotechnics*, *20*(1), 24–37. https://doi.org/10.1680/jphmg.18.00031

Steward, J. E. (n.d.). *Launched Soil Nails: New Method for Rapid Low-Impact Slope Repairs*.

Stutz, H. H., & Martinez, A. (2021). Directionally dependent strength and dilatancy behavior of soil–structure interfaces. *Acta Geotechnica*, *16*(9), 2805–2820. https://doi.org/10.1007/s11440-021-01199-5

Tei, K., Taylor, R.N., & Milligan, G.W.E. (1998). Centrifuge Model Tests of Nailed Soil Slopes. *Soils and Foundations, 38(2), 165-177.*

Uesugi, M., & Kishida, H. (1986). Frictional Resistance at Field Between Dry Sand and Mild Steel. *Soils and Foundations, 26(4) 139-149.*

Wang, Q., Ye, X., Wang, S., Sloan, S. W., & Sheng, D. (2017). Experimental investigation of compaction-grouted soil nails. *Canadian Geotechnical Journal*, *54*(12), 1728–1738. https://doi.org/10.1139/cgj-2017-0063

Wang, Z., & Richwien, W. (2002). A Study of Soil-Reinforcement Interface Friction. *Journal of Geotechnical and Geoenvironmental Engineering*, *128*(1), 92–94. https://doi.org/10.1061/(ASCE)1090-0241(2002)128:1(92)

White, D.J., and Lehane, B.M. (2004). Friction fatigue on displacement piles in sand. *Géotechnique*, 54(10), 645-658. https://doi.org/10.1680/geot.2004.54.10.645

Xu, D. S., Liu, H. B., & Luo, W. L. (2018). Evaluation of interface shear behavior of GFRP soil nails with a strain-transfer model and distributed fiber-optic sensors. *Computers and Geotechnics*, *95*, 180–190. https://doi.org/10.1016/j.compgeo.2017.10.005

Zhang, L. L., Zhang, L. M., & Tang, W. H. (2009). Uncertainties of Field Pullout Resistance of Soil Nails. *Journal of Geotechnical and Geoenvironmental Engineering*, *135*(7), 966–972. https://doi.org/10.1061/(ASCE)GT.1943-5606.0000014

Zhong, W., Liu, H., Wang, Q., Zhang, W., Li, Y., Ding, X., & Chen, L. (2021). Investigation of the penetration characteristics of snake skin-inspired pile using DEM. *Acta Geotechnica*, *16*(6), 1849–1865. https://doi.org/10.1007/s11440-020-01132-2

Zhu, H.-H., Yin, J.-H., Yeung, A. T., & Jin, W. (2011). Field Pullout Testing and Performance Evaluation of GFRP Soil Nails. *Journal of Geotechnical and Geoenvironmental Engineering*, *137*(7), 633–642. https://doi.org/10.1061/(ASCE)GT.1943-5606.0000457

Table 1: Asperity dimensions of the snakeskin-inspired anchors.

Designation	Asperity height, H (mm)	Asperity length, L (mm)	Geometry ratio, L/H
H4L12	4	12	3
H2L12	2	12	6
H1L12	1	12	12
H0.5L12	0.5	12	24
H4L24	4	24	6
H2L24	2	24	12
H4L48	4	48	12
H2L48	2	48	24

Table 2: Results of anchor load tests in the sand pit site.

Designa-tion	Asperity height, H (mm)	Asperity length, L (mm)	Geo-metry ratio, L/H	Tip depth, z (m)	Avg. initial eff. stress, σ'_v (kPa)	Install. load at 1.3 m (kN)	Install. shaft force at 1.3 m (kN)	Peak pullout force (kN)	Peak pullout stress ratio, τ_{peak}/σ'_v	Peak directio-nality
H4L12	4	12	3	1.3	12.4	11.4	8.1	11.6	11.1	1.4
H2L12	2	12	6	2.2	21.6	6.6	3.1	15.0	4.6	2.0
H1L12	1	12	12	2.3	22.7	5.9	2.4	12.9	3.7	2.7
H0.5L12	0.5	12	24	2.3	22.6	3.7	0.7	11.4	3.2	2.9
H4L24	4	24	6	1.9	18.6	9.8	6.7	15.7	6.7	1.8
H2L24	2	24	12	2.5	24.1	6.0	2.6	12.8	3.6	2.2
H4L48	4	48	12	2.2	21.5	7.8	4.2	13.9	5.1	1.8
H2L48	2	48	24	2.3	22.1	5.4	1.5	9.1	2.9	2.2
Rebar	-	-	-	2.0	19.2	-	-	7.7	2.6	-

Table 3: Results of anchor load tests in the Yolo loam site.

Designa-tion	Asperity height, H (mm)	Asperity length, L (mm)	Geo-metry ratio, L/H	Tip depth, z (m)	Avg. initial eff. stress, σ'_v (kPa)	Install. load (kN)[a]	Install. shaft force (kN)[b]	Peak pullout force (kN)	Peak pullout stress ratio, τ_{peak}/σ'_v	Peak directio-nality
H4L12	4	12	3	2.5	22.6	1.8	0.7	0.4	0.1	0.2
H2L12	2	12	6	2.7	24.4	1.7	0.6	1.3	0.4	0.9
H1L12	1	12	12	2.4	22.0	2.8	1.6	3.4	1.0	1.7
H0.5L12	0.5	12	24	2.6	23.8	3.0	1.8	6.3	1.5	2.3
H4L24	4	24	6	2.7	24.2	1.6	0.4	0.3	0.1	0.2
H2L24	2	24	12	2.8	25.2	1.8	0.7	1.4	0.4	1.0
H4L48	4	48	12	2.8	25.2	1.7	0.7	1.0	0.3	0.9
H2L48	2	48	24	2.7	24.4	1.5	0.5	2.0	0.6	0.7
Rebar	-	-	-	2.7	24.4	-	-	2.9	0.6	-
H4L12	4	12	3	5.6	50.6	3.7	2.1	3.6	0.3	0.9
H2L12	2	12	6	5.3	48.0	3.8	2.1	4.0	0.2	1.2
H1L12	1	12	12	5.5	49.4	3.3	1.5	6.8	0.4	3.1
H0.5L12	0.5	12	24	4.8	43.6	4.8	2.7	17.4	1.3	4.5
H4L24	4	24	6	5.6	50.7	1.9	0.0	1.7	0.1	0.8
H2L24	2	24	12	5.1	46.4	2.7	0.9	3.2	0.2	1.6
H4L48	4	48	12	5.0	44.8	2.9	0.8	1.4	0.1	0.6
H2L48	2	48	24	5.4	48.9	2.8	1.3	3.5	0.2	1.6
Rebar	-	-	-	5.5	48.9	-	-	5.3	0.3	-

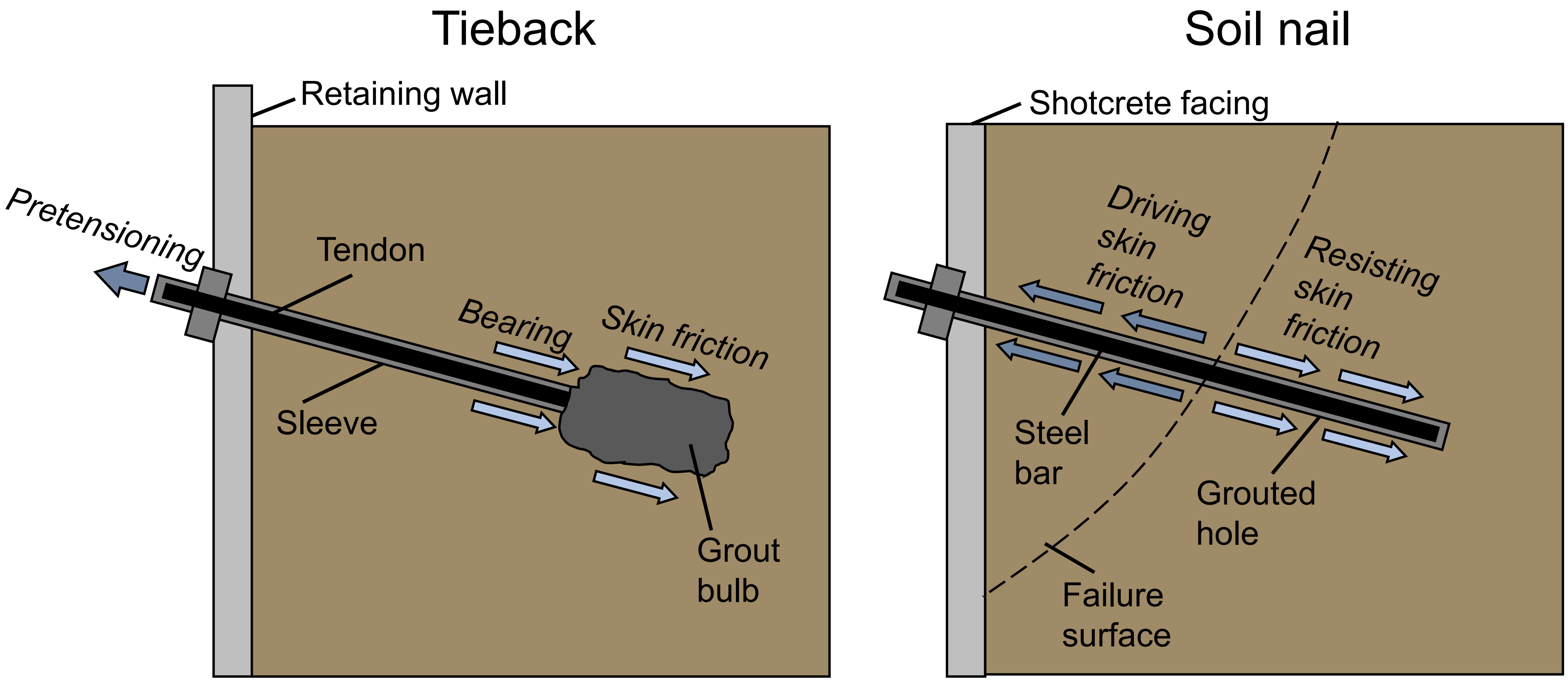
Tieback
Retaining wall
Pretensioning
Tendon
Bearing
Skin friction
Sleeve
Grout
bulb
Soil nail
Shotcrete facing
Driving
skin
friction
Resisting
skin
friction
Steel
bar
Grouted
hole
Failure
surface

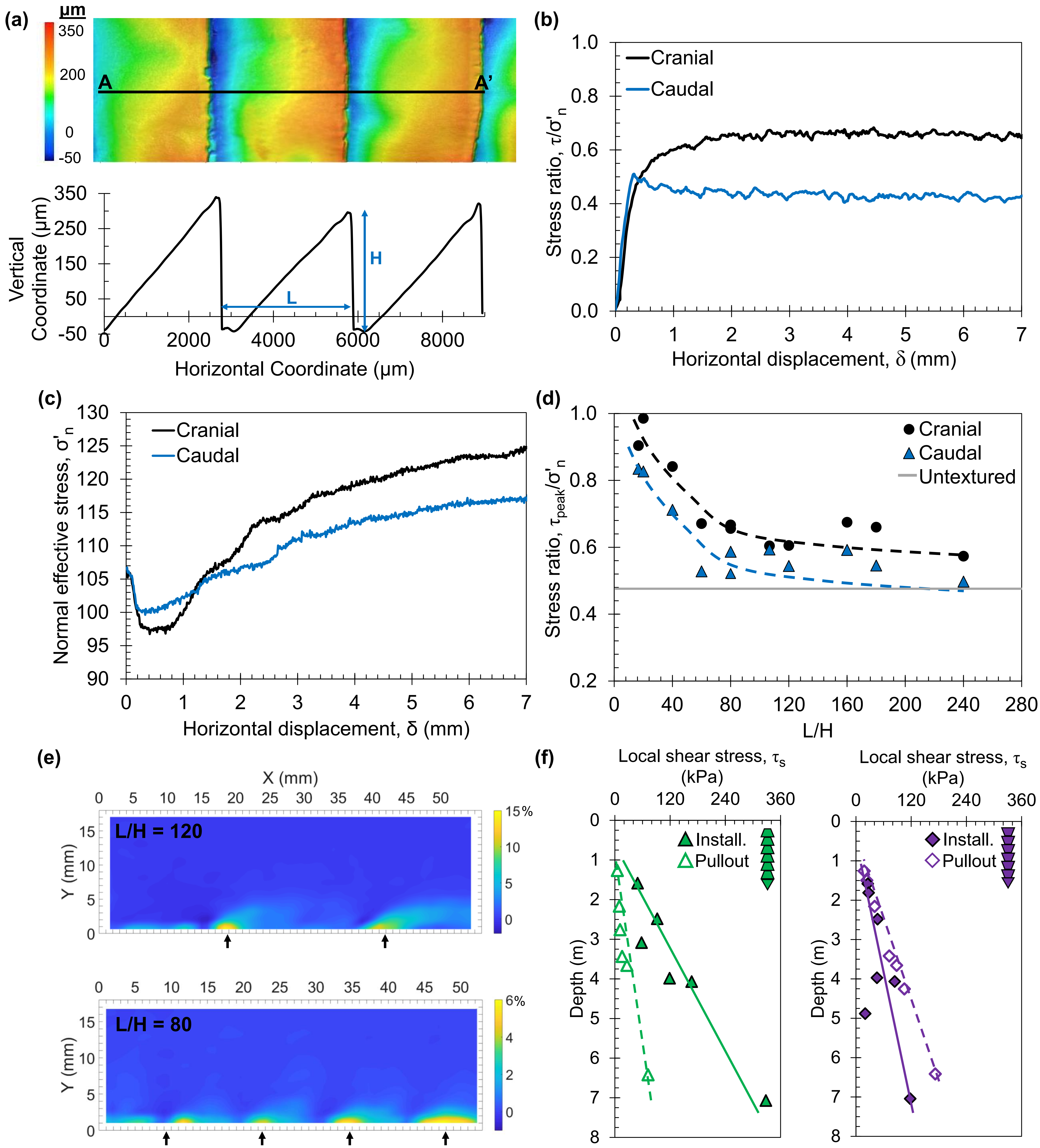

(a)
μm
350
200
0
-50
A
A'
Vertical Coordinate (μm)
Horizontal Coordinate (μm)
H
L
(b)
Cranial
Caudal
Stress ratio, τ/σ'n
Horizontal displacement, δ (mm)
(c)
Cranial
Caudal
Normal effective stress, σ'n
Horizontal displacement, δ (mm)
(d)
Cranial
Caudal
Untextured
Stress ratio, τpeak/σ'n
L/H
(e)
X (mm)
Y (mm)
L/H = 120
15%
L/H = 80
6%
(f)
Local shear stress, τs (kPa)
Depth (m)
Install.
Pullout

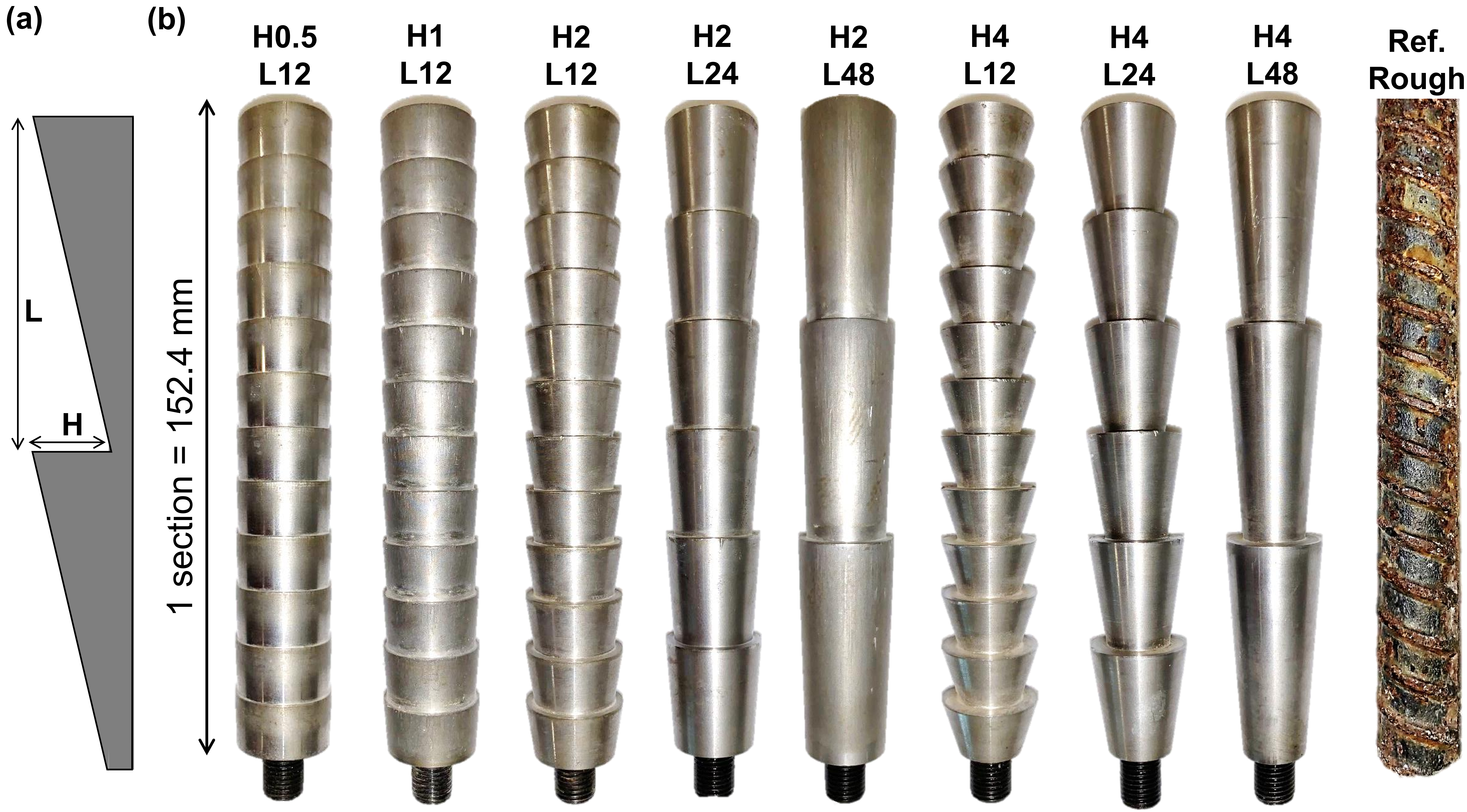

(a)
(b)
H0.5
L12
H1
L12
H2
L12
H2
L24
H2
L48
H4
L12
H4
L24
H4
L48
Ref.
Rough
L
H
1 section = 152.4 mm

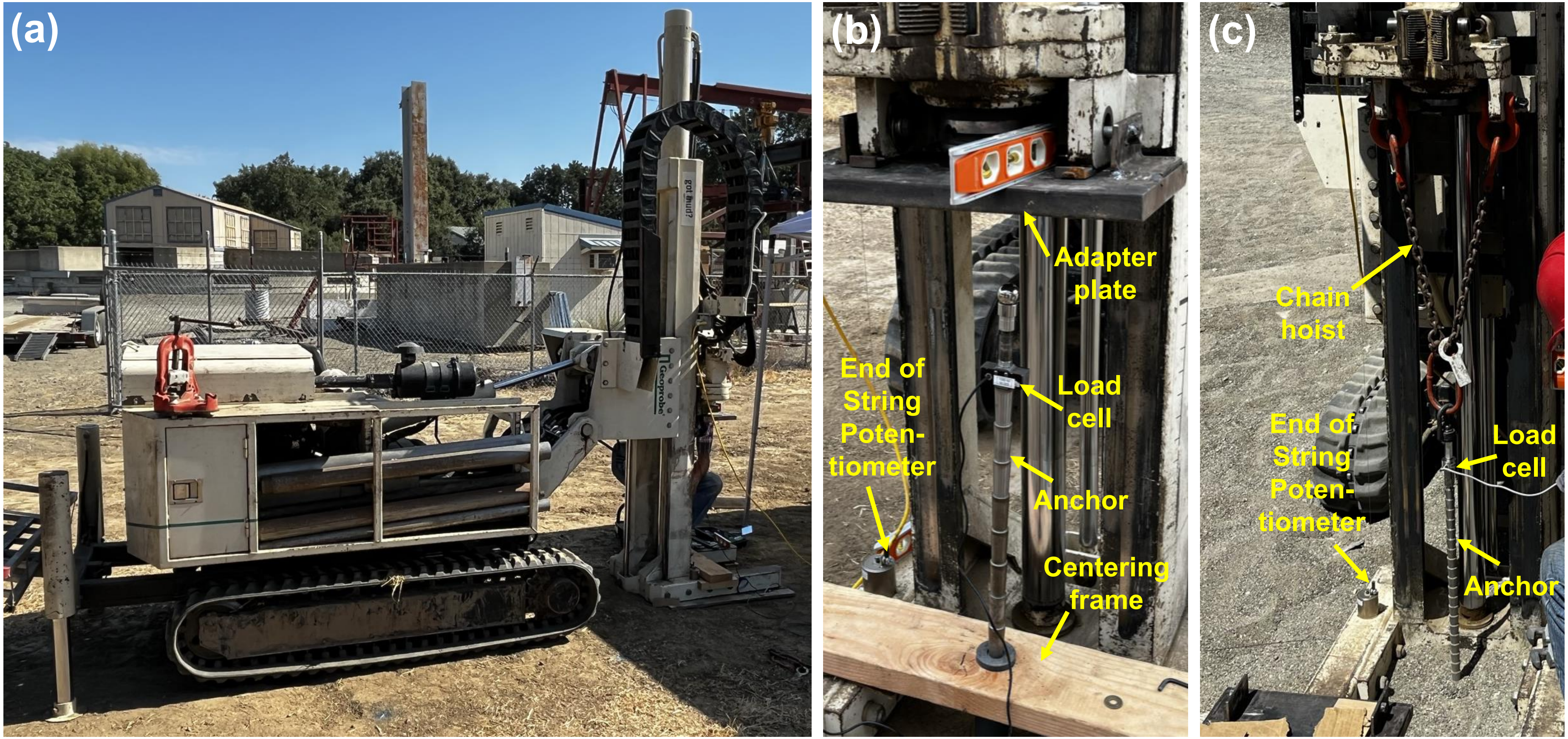

(a)
got mud?
Geoprobe
(b)
Adapter plate
Load cell
Anchor
End of String Poten-tiometer
Centering frame
(c)
Chain hoist
End of String Poten-tiometer
Load cell
Anchor

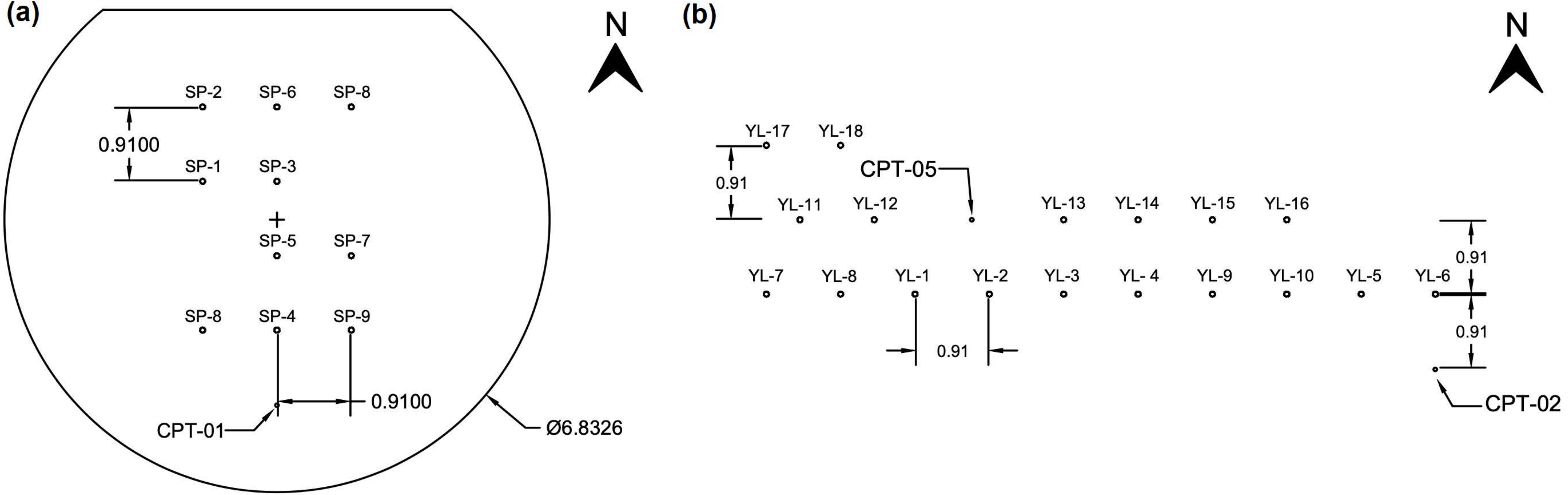

(a)
N
SP-2
SP-6
SP-8
0.9100
SP-1
SP-3
SP-5
SP-7
SP-8
SP-4
SP-9
0.9100
CPT-01
Ø6.8326
(b)
N
YL-17
YL-18
CPT-05
0.91
YL-11
YL-12
YL-13
YL-14
YL-15
YL-16
0.91
YL-7
YL-8
YL-1
YL-2
YL-3
YL- 4
YL-9
YL-10
YL-5
YL-6
0.91
0.91
CPT-02

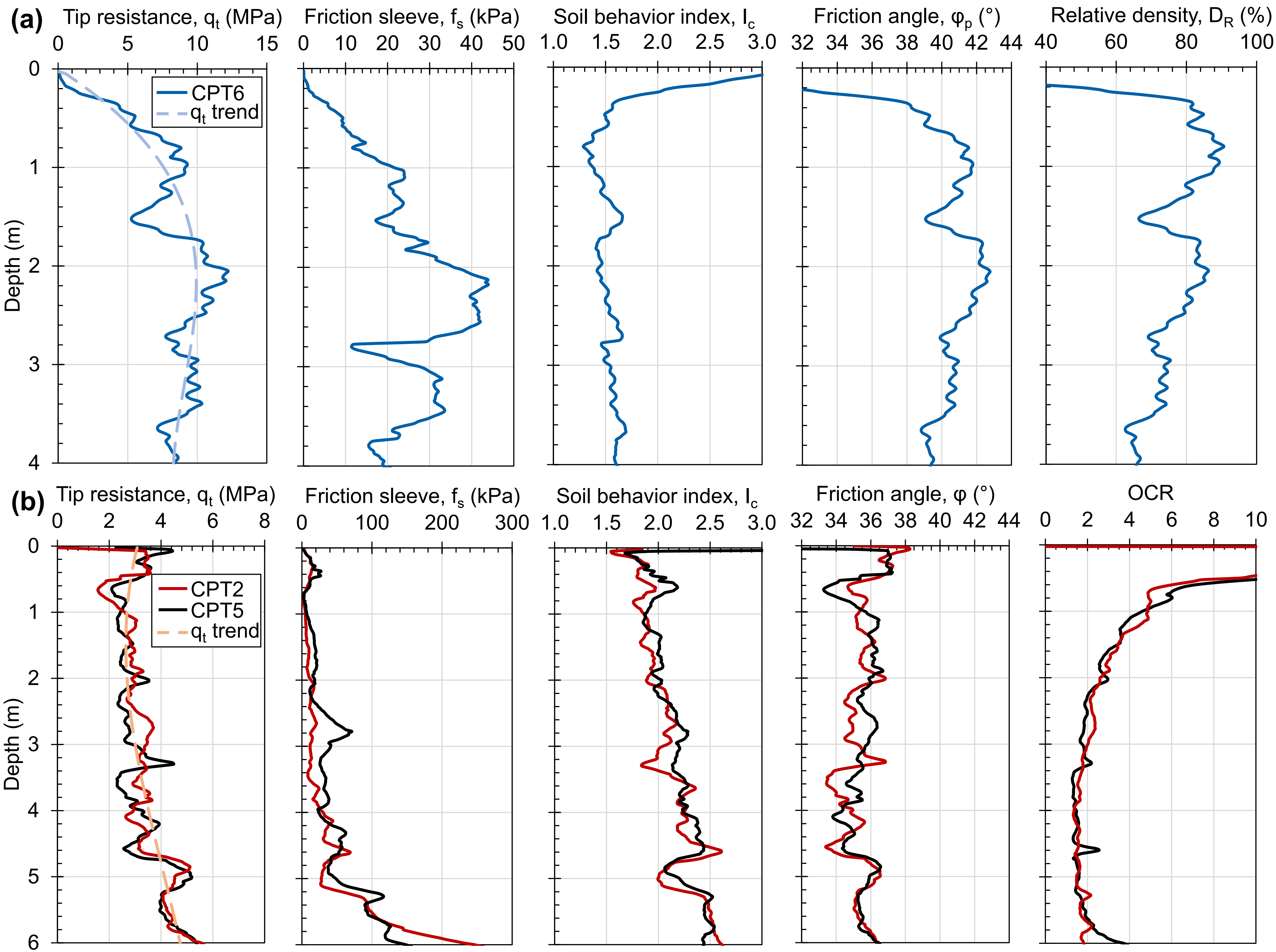

(a)
Tip resistance, q_t (MPa)
Friction sleeve, f_s (kPa)
Soil behavior index, I_c
Friction angle, φ_p (°)
Relative density, D_R (%)
Depth (m)
CPT6
q_t trend
(b)
Tip resistance, q_t (MPa)
Friction sleeve, f_s (kPa)
Soil behavior index, I_c
Friction angle, φ (°)
OCR
Depth (m)
CPT2
CPT5
q_t trend

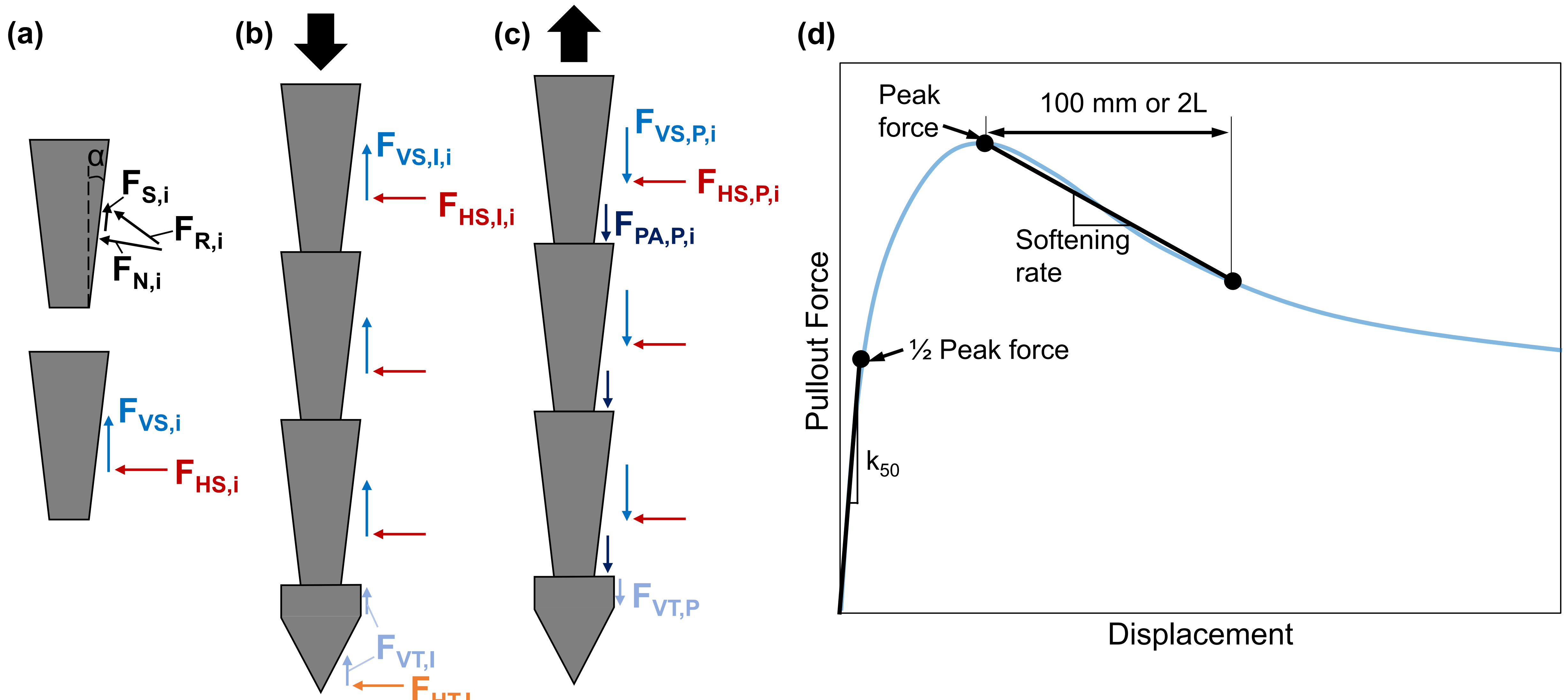

(a)
α
F S,i
F R,i
F N,i
F VS,i
F HS,i
(b)
F VS,I,i
F HS,I,i
F VT,I
F HT,I
(c)
F VS,P,i
F HS,P,i
F PA,P,i
F VT,P
(d)
Peak force
100 mm or 2L
Softening rate
½ Peak force
k50
Pullout Force
Displacement

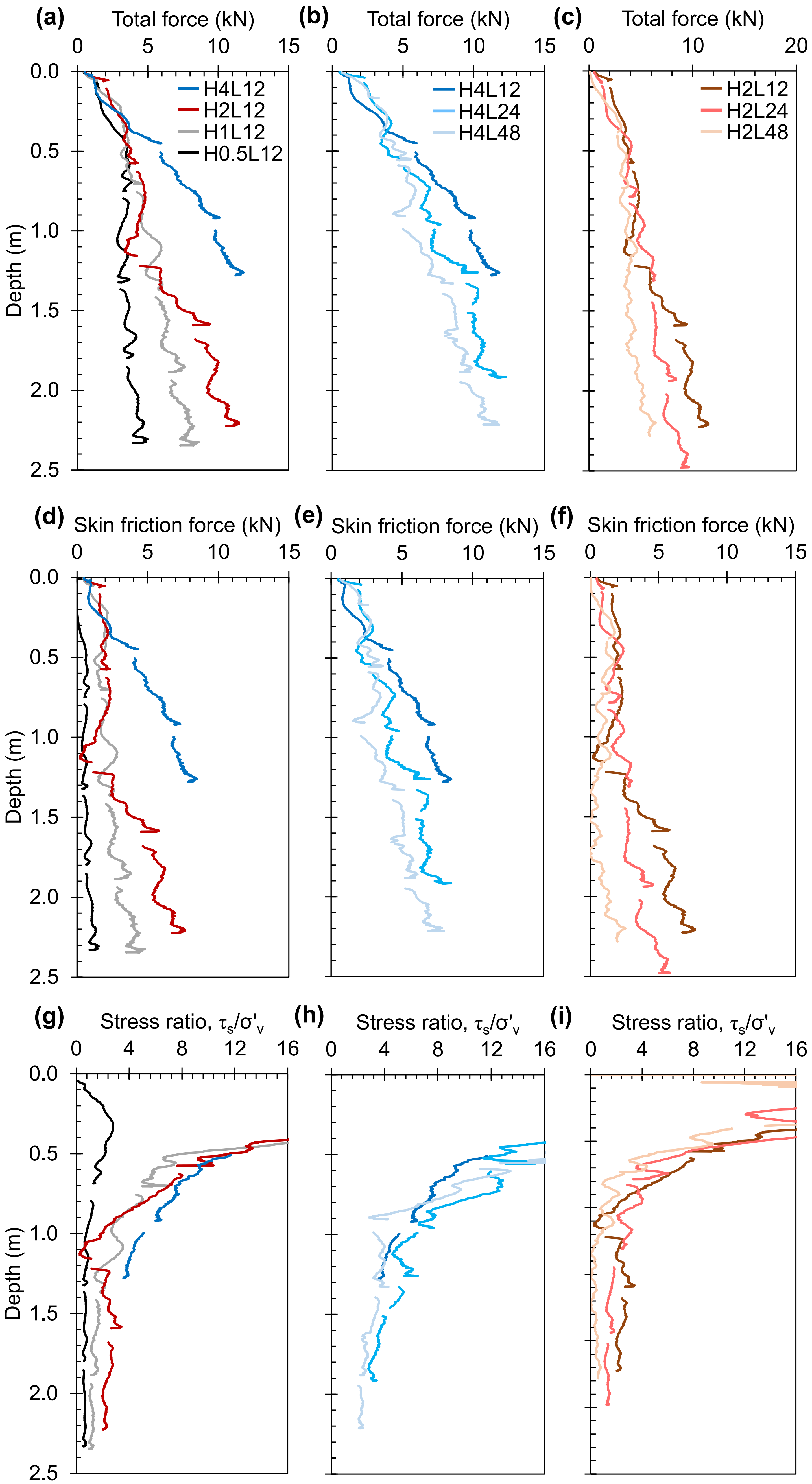

(a)
Total force (kN)
0
5
10
15
Depth (m)
0.0
0.5
1.0
1.5
2.0
2.5
H4L12
H2L12
H1L12
H0.5L12
(b)
Total force (kN)
H4L12
H4L24
H4L48
(c)
Total force (kN)
0
10
20
H2L12
H2L24
H2L48
(d)
Skin friction force (kN)
(e)
Skin friction force (kN)
(f)
Skin friction force (kN)
(g)
Stress ratio, τs/σ'v
0
4
8
12
16
(h)
Stress ratio, τs/σ'v
(i)
Stress ratio, τs/σ'v

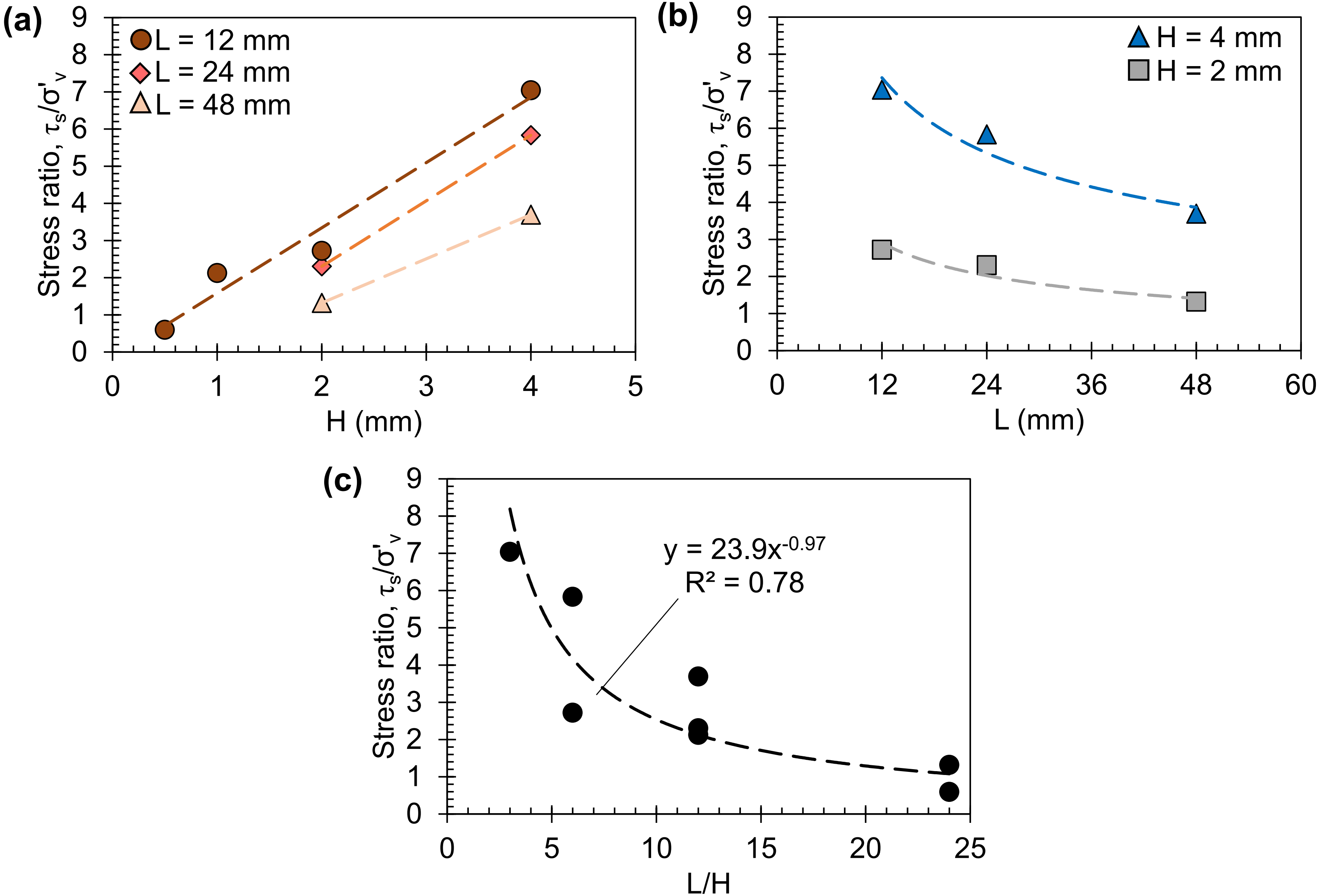

(a)
L = 12 mm
L = 24 mm
L = 48 mm
Stress ratio, τs/σ'v
H (mm)
(b)
H = 4 mm
H = 2 mm
Stress ratio, τs/σ'v
L (mm)
(c)
y = 23.9x-0.97
R² = 0.78
Stress ratio, τs/σ'v
L/H

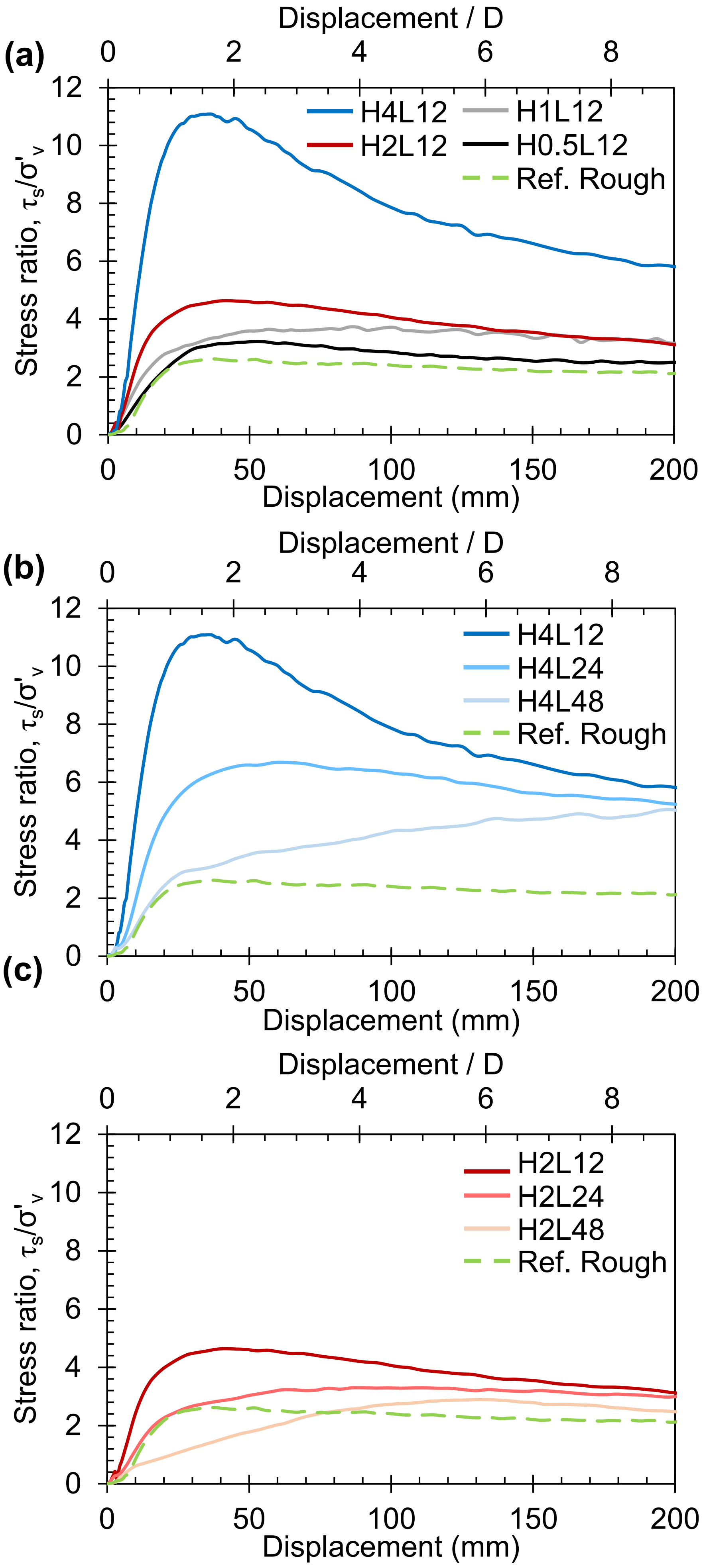
(a)
Displacement / D
0
2
4
6
8
Stress ratio, τs/σ'v
0
2
4
6
8
10
12
H4L12
H2L12
H1L12
H0.5L12
Ref. Rough
0
50
100
150
200
Displacement (mm)
(b)
Displacement / D
H4L12
H4L24
H4L48
Ref. Rough
Displacement (mm)
(c)
Displacement / D
H2L12
H2L24
H2L48
Ref. Rough
Displacement (mm)

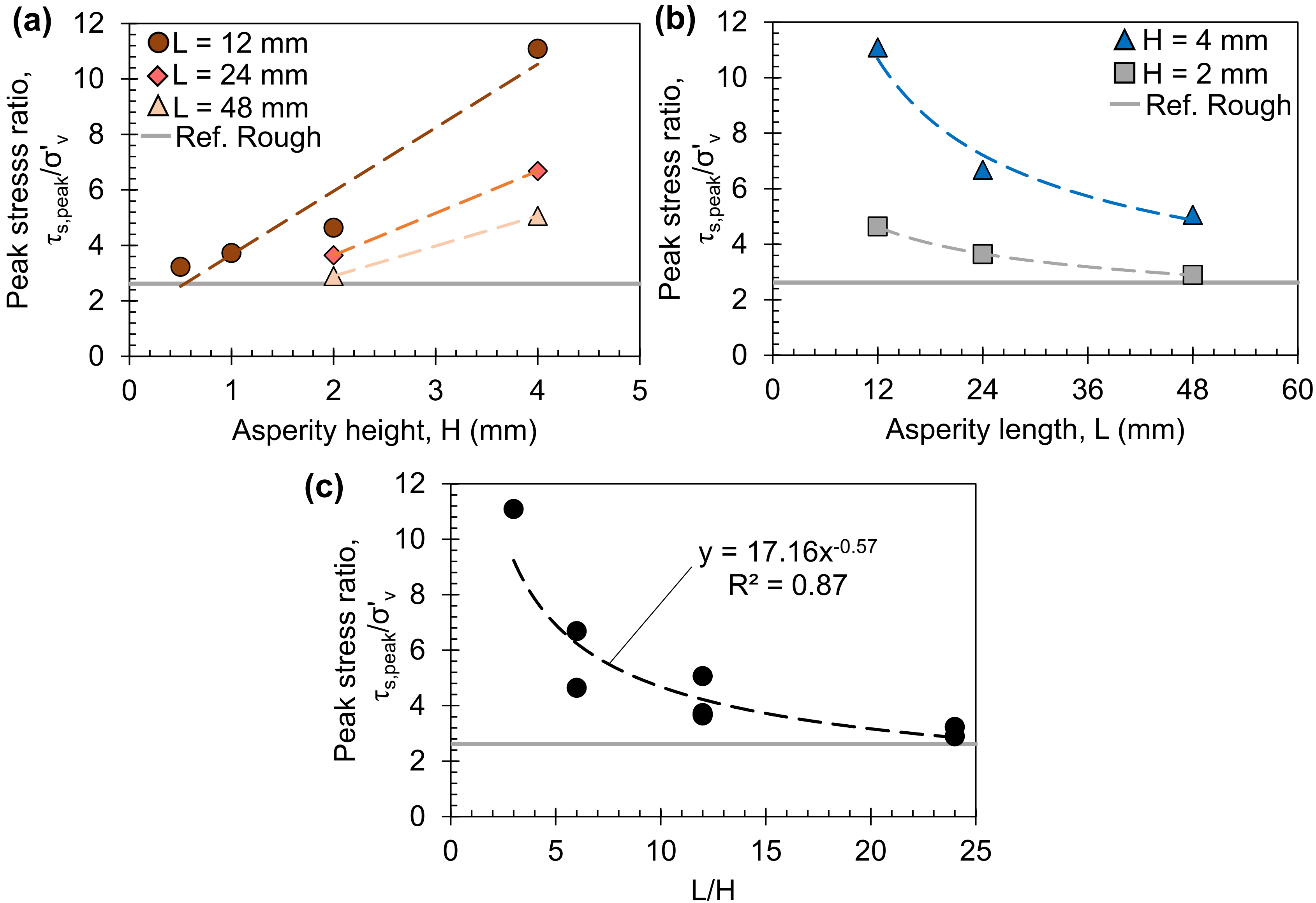

(a)
Peak stresss ratio, $\tau_{s,peak}/\sigma'_v$
L = 12 mm
L = 24 mm
L = 48 mm
Ref. Rough
Asperity height, H (mm)
(b)
Peak stress ratio, $\tau_{s,peak}/\sigma'_v$
H = 4 mm
H = 2 mm
Ref. Rough
Asperity length, L (mm)
(c)
Peak stress ratio, $\tau_{s,peak}/\sigma'_v$
$y = 17.16x^{-0.57}$
$R^2 = 0.87$
L/H

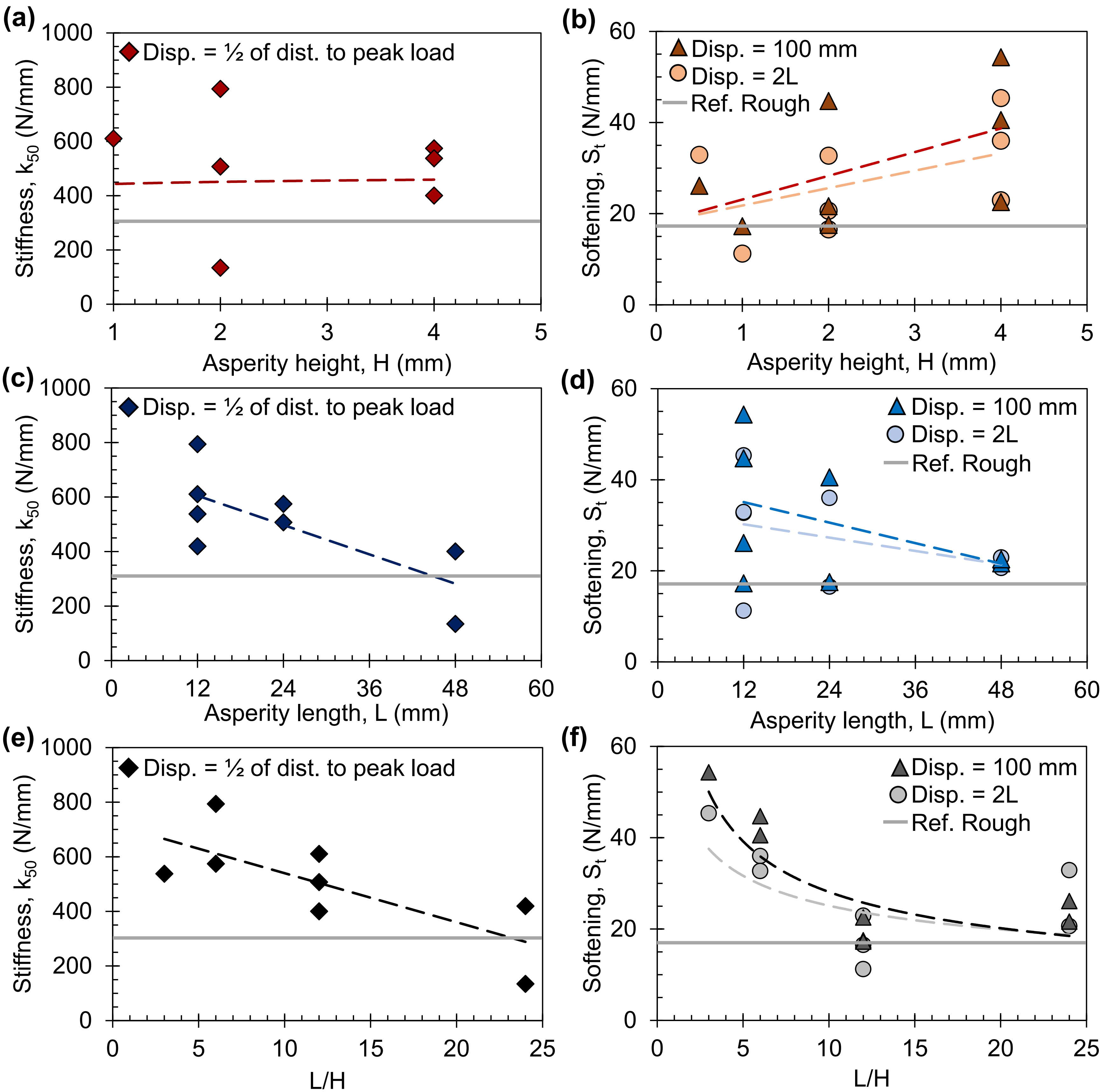

(a)
Disp. = ½ of dist. to peak load
Stiffness, k50 (N/mm)
Asperity height, H (mm)
(b)
Disp. = 100 mm
Disp. = 2L
Ref. Rough
Softening, St (N/mm)
Asperity height, H (mm)
(c)
Disp. = ½ of dist. to peak load
Stiffness, k50 (N/mm)
Asperity length, L (mm)
(d)
Disp. = 100 mm
Disp. = 2L
Ref. Rough
Softening, St (N/mm)
Asperity length, L (mm)
(e)
Disp. = ½ of dist. to peak load
Stiffness, k50 (N/mm)
L/H
(f)
Disp. = 100 mm
Disp. = 2L
Ref. Rough
Softening, St (N/mm)
L/H

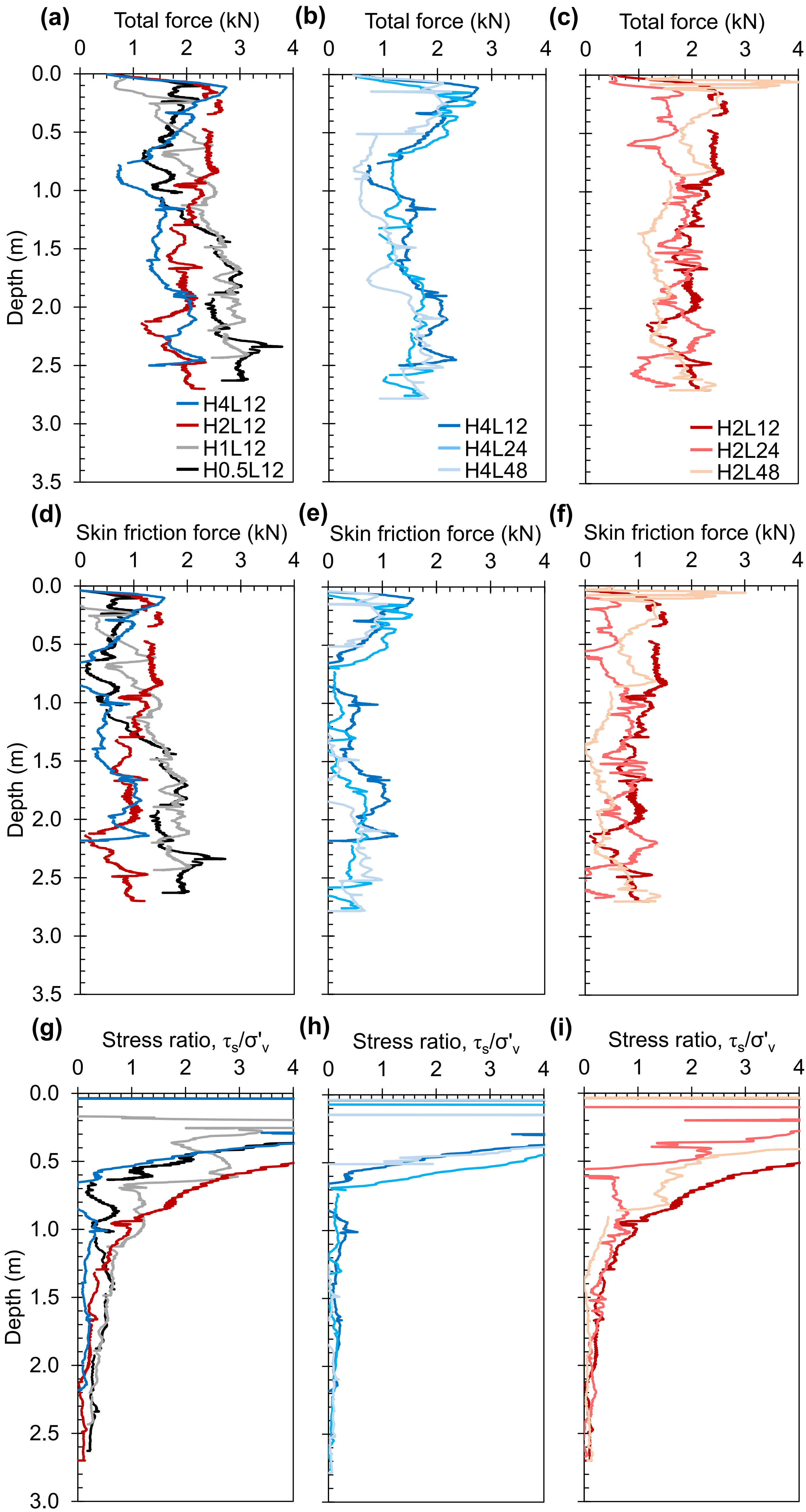
(a)
Total force (kN)
(b)
Total force (kN)
(c)
Total force (kN)
Depth (m)
H4L12
H2L12
H1L12
H0.5L12
H4L12
H4L24
H4L48
H2L12
H2L24
H2L48
(d)
Skin friction force (kN)
(e)
Skin friction force (kN)
(f)
Skin friction force (kN)
Depth (m)
(g)
Stress ratio, τ_s/σ'_v
(h)
Stress ratio, τ_s/σ'_v
(i)
Stress ratio, τ_s/σ'_v
Depth (m)

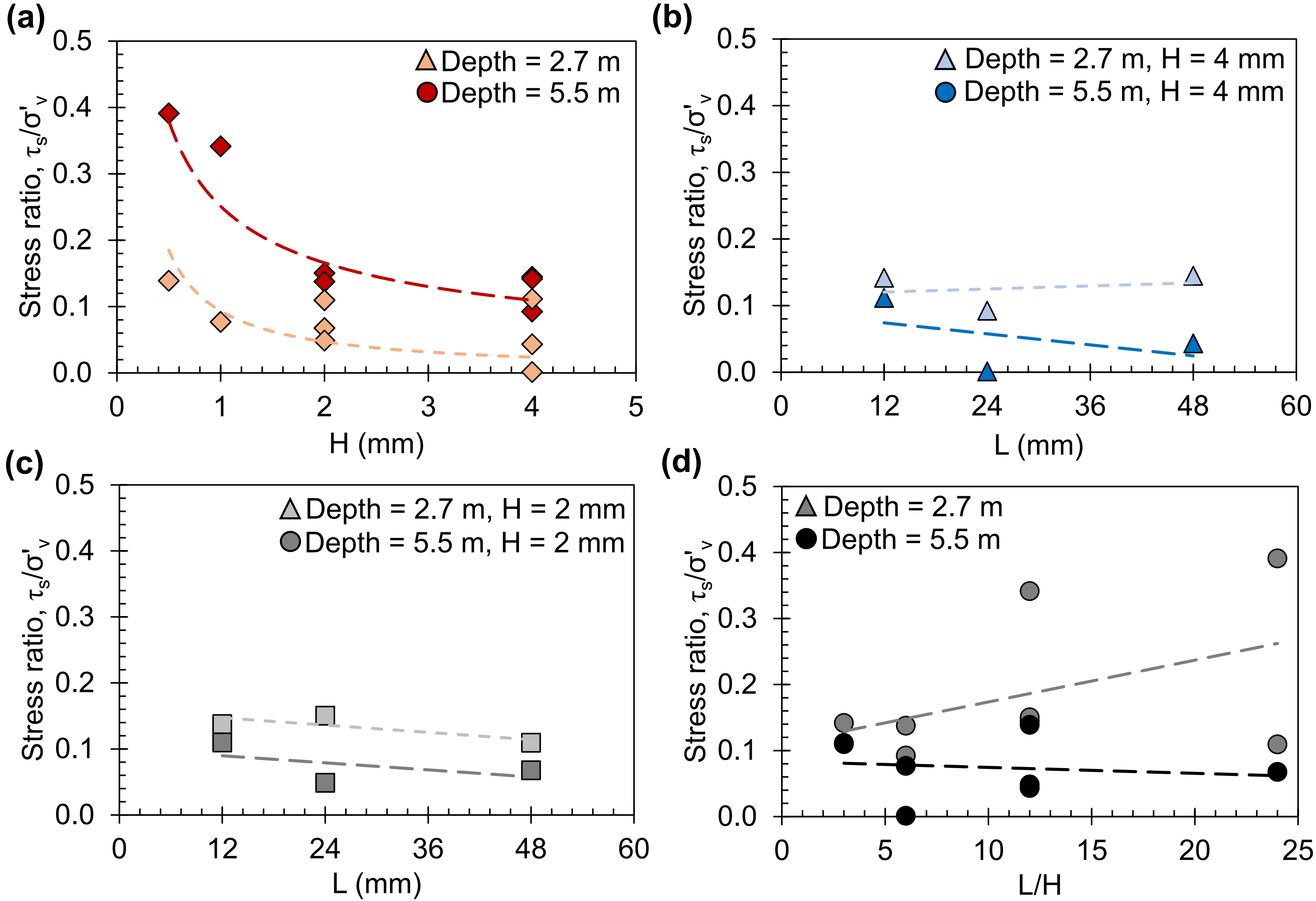

(a)
Depth = 2.7 m
Depth = 5.5 m
Stress ratio, τs/σ'v
H (mm)
(b)
Depth = 2.7 m, H = 4 mm
Depth = 5.5 m, H = 4 mm
Stress ratio, τs/σ'v
L (mm)
(c)
Depth = 2.7 m, H = 2 mm
Depth = 5.5 m, H = 2 mm
Stress ratio, τs/σ'v
L (mm)
(d)
Depth = 2.7 m
Depth = 5.5 m
Stress ratio, τs/σ'v
L/H

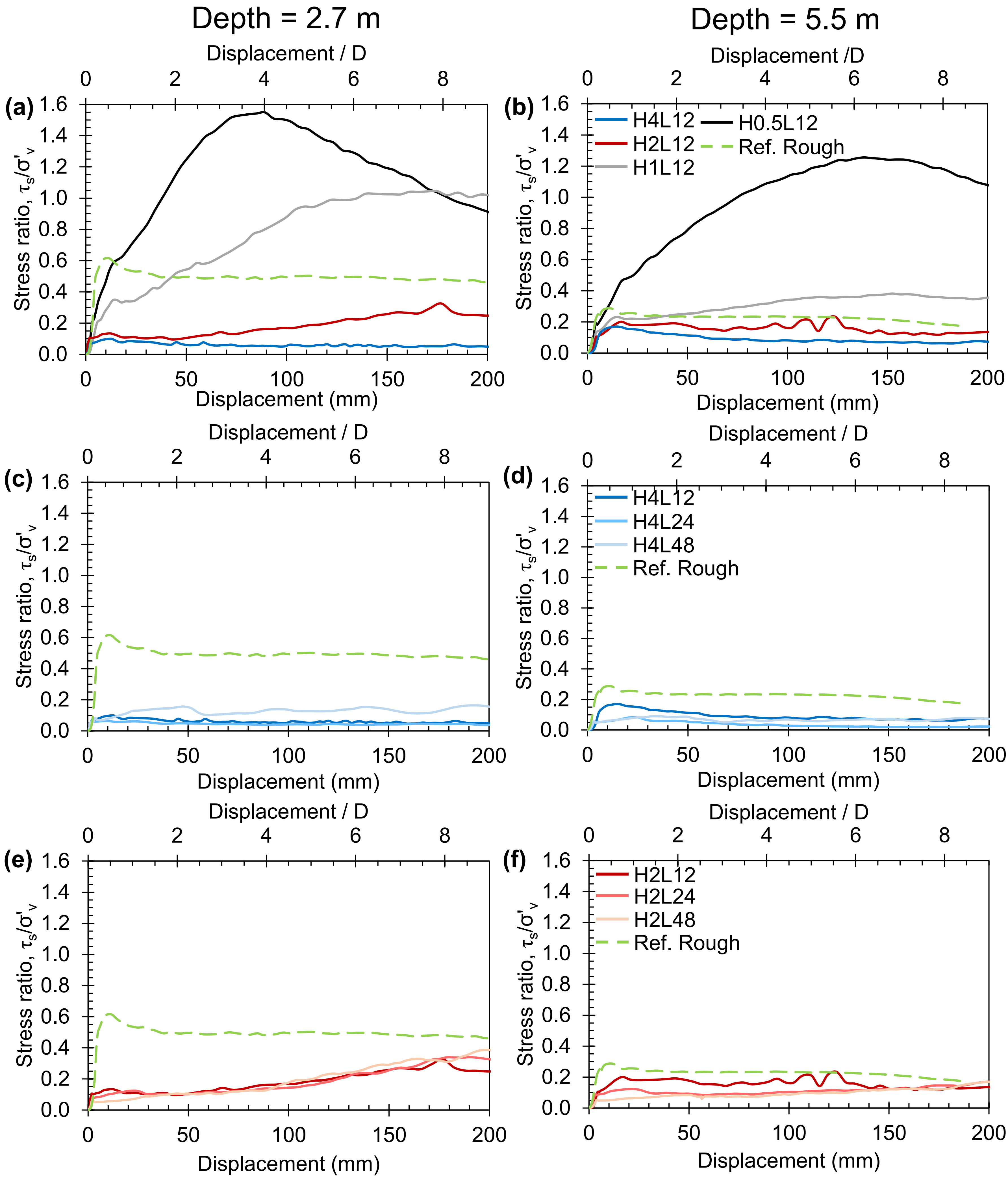

Depth = 2.7 m
Depth = 5.5 m
Displacement / D
Displacement /D
(a)
(b)
(c)
(d)
(e)
(f)
Stress ratio, τ_s/σ'_v
Displacement (mm)
H4L12
H2L12
H1L12
H0.5L12
Ref. Rough
H4L24
H4L48
H2L24
H2L48

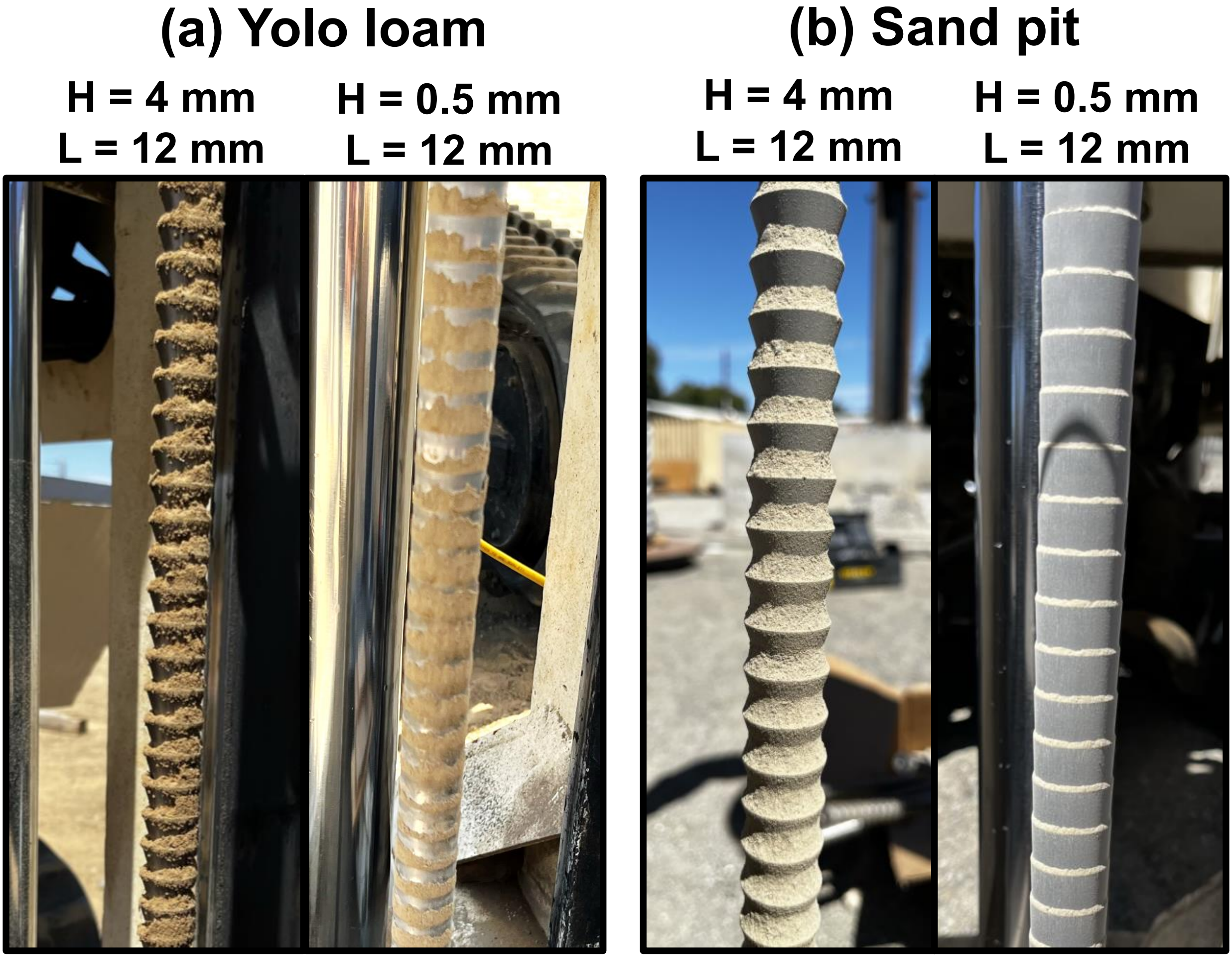
(a) Yolo loam
H = 4 mm
L = 12 mm
H = 0.5 mm
L = 12 mm
(b) Sand pit
H = 4 mm
L = 12 mm
H = 0.5 mm
L = 12 mm

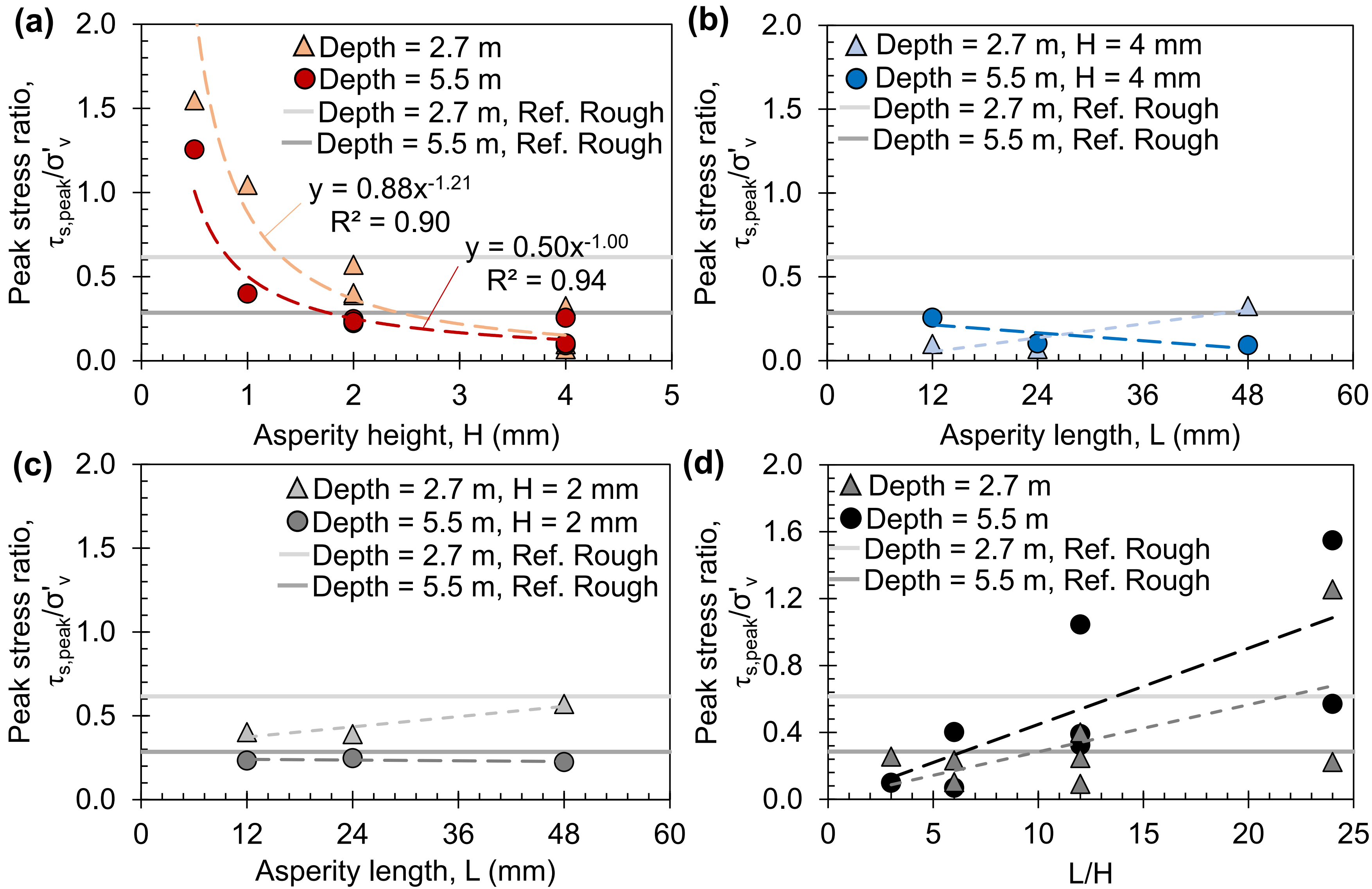

(a)
Depth = 2.7 m
Depth = 5.5 m
Depth = 2.7 m, Ref. Rough
Depth = 5.5 m, Ref. Rough
y = 0.88x^-1.21
R² = 0.90
y = 0.50x^-1.00
R² = 0.94
Peak stress ratio, τs,peak/σ'v
Asperity height, H (mm)
(b)
Depth = 2.7 m, H = 4 mm
Depth = 5.5 m, H = 4 mm
Depth = 2.7 m, Ref. Rough
Depth = 5.5 m, Ref. Rough
Peak stress ratio, τs,peak/σ'v
Asperity length, L (mm)
(c)
Depth = 2.7 m, H = 2 mm
Depth = 5.5 m, H = 2 mm
Depth = 2.7 m, Ref. Rough
Depth = 5.5 m, Ref. Rough
Peak stress ratio, τs,peak/σ'v
Asperity length, L (mm)
(d)
Depth = 2.7 m
Depth = 5.5 m
Depth = 2.7 m, Ref. Rough
Depth = 5.5 m, Ref. Rough
Peak stress ratio, τs,peak/σ'v
L/H

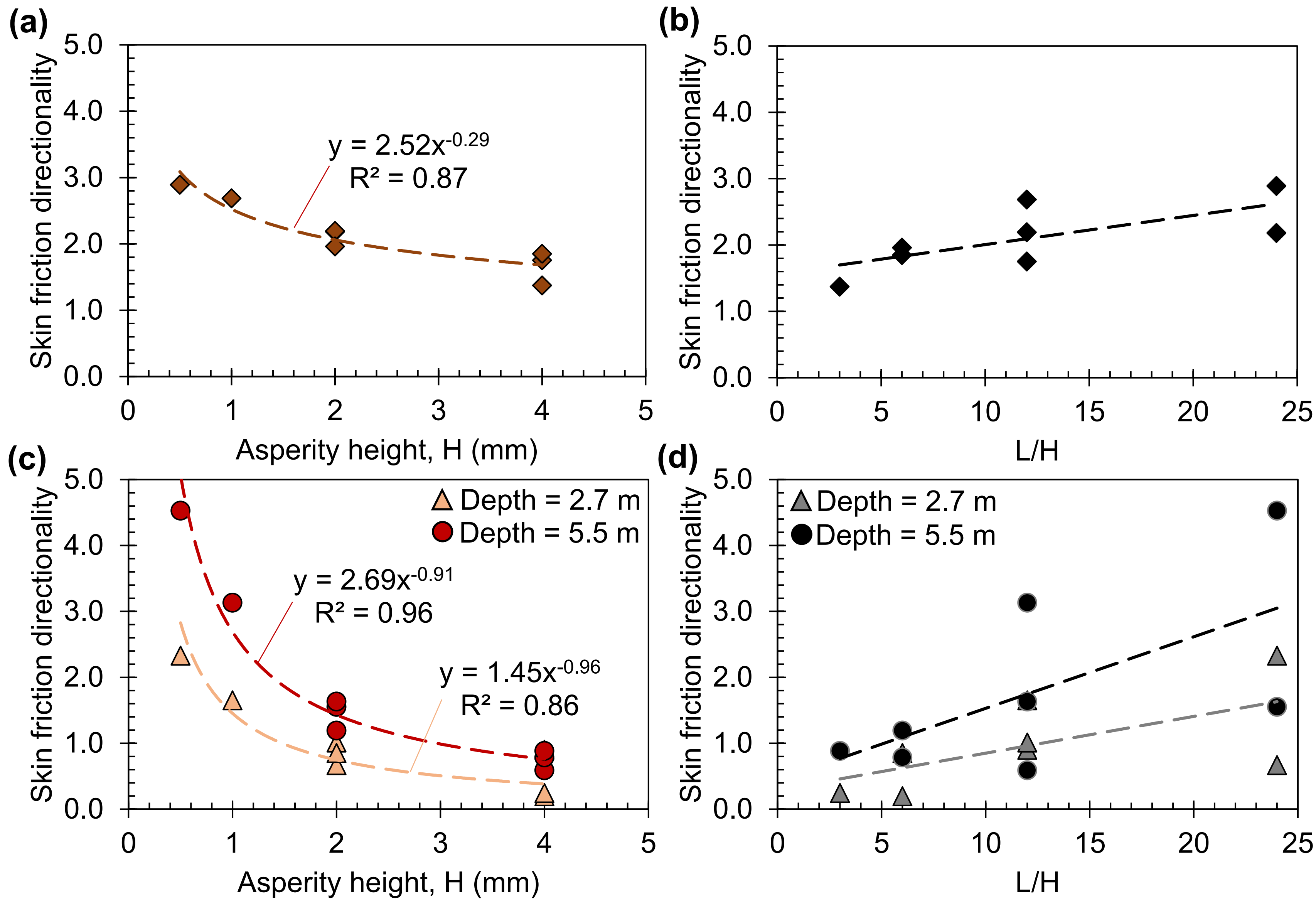

(a)
y = 2.52x^-0.29
R² = 0.87
Skin friction directionality
Asperity height, H (mm)
(b)
Skin friction directionality
L/H
(c)
Depth = 2.7 m
Depth = 5.5 m
y = 2.69x^-0.91
R² = 0.96
y = 1.45x^-0.96
R² = 0.86
Skin friction directionality
Asperity height, H (mm)
(d)
Depth = 2.7 m
Depth = 5.5 m
Skin friction directionality
L/H